Antioxidants and Redox Signaling

DOI: 10.1089/ars.2016.6748

Mesenchymal stem cell therapy protects lungs from radiation-induced endothelial cell loss by restoring superoxide dismutase 1 expression (doi: 10.1089/ars.2016.6748)
This paper has been peer-reviewed and accepted for publication, but has yet to undergo copyediting and proof correction. The final published version may differ from this proof.

Original Research Communication

Running head: Radioprotection of lung EC

Mesenchymal stem cell therapy protects lungs from radiation-induced endothelial cell loss by restoring superoxide dismutase 1 expression

Diana Klein[1], Jennifer Steens[1], Alina Wiesemann[1], Florian Schulz[2], Farnusch Kaschani[2], Katharina Röck[3], Masahiro Yamaguchi[4], Florian Wirsdörfer[1], Markus Kaiser[2], Jens W. Fischer[3], Martin Stuschke[5], Verena Jendrossek[1]

[1]Institute of Cell Biology (Cancer Research), University of Duisburg-Essen, University Hospital, 45122 Essen, Germany.
[2]Department of Chemical Biology, University of Duisburg-Essen, Center for Medical Biotechnology, Faculty of Biology, 45117 Essen, Germany.
[3]Institute for Pharmacology, University Hospital, Heinrich-Heine-University, 40225 Düsseldorf, Germany
[4]Department of Physiology, Kochi Medical School, Kochi, Japan
[5]Department of Radiotherapy, University of Duisburg-Essen, University Hospital, 45122 Essen, Germany
Department of Physiology,

Correspondence to

PD Dr. rer. nat. Diana Klein
Institute of Cell Biology (Cancer Research)
University Hospital Essen, University of Duisburg-Essen
Virchowstr. 173, Ger-45147 Essen
Tel: +49-201-723 83342; Fax: +49-201-723 5904
E-mail: Diana.Klein@uk-essen.de

Word count (excluding References and Figure legends):7621

Reference number: 87

Number of grey scale illustrations for print version: 9 (Figure 1-9)

Number of color illustrations for online version: 7 (Figure 2, 3, 5, 6, 7, 8, 9)

Abstract (247 words)

Aims: Radiation-induced normal tissue toxicity is closely linked to endothelial cell (EC) damage and dysfunction (acute effects). However, the underlying mechanisms of radiation-induced adverse late effects with respect to the vascular compartment remain elusive and no causative radioprotective treatment is available to date.

Results:

The importance of injury to EC for radiation-induced late toxicity in lungs after whole thorax irradiation (WTI) was investigated using a mouse model of radiation-induced pneumopathy. We show that WTI induces EC loss as long-term complication which is accompanied by the development of fibrosis. Adoptive transfer of mesenchymal stem cells (MSCs) either derived from bone marrow or aorta (vascular wall-resident MSCs) in the early phase after irradiation limited the radiation-induced EC loss and fibrosis progression. Furthermore, MSC-derived culture supernatants rescued the radiation-induced reduction in viability and long-term survival of cultured lung EC. We further identified the antioxidant enzyme superoxide dismutase 1 (SOD1) as MSC-secreted factor. Importantly, MSC-treatment restored the radiation-induced reduction of SOD1 levels after WTI. A similar protective effect was achieved by using the SOD-mimitic EUK134 suggesting that MSC-derived SOD1 is involved in the protective action of MSC presumably though paracrine signaling.

Innovation:

Here we explored the therapeutic potential of MSC therapy to prevent radiation-induced EC loss (late effect) and identified the protective mechanisms of MSC action.

Conclusions:

Adoptive transfer of MSCs early after irradiation counteracts radiation-induced vascular damage and EC loss as late adverse effects. The high activity of vascular wall-derived MSCs for radioprotection may be due to their tissue-specific action.

Mesenchymal stem cell therapy protects lungs from radiation-induced endothelial cell loss by restoring superoxide dismutase 1 expression (doi: 10.1089/ars.2016.6748)
This paper has been peer-reviewed and accepted for publication, but has yet to undergo copyediting and proof correction. The final published version may differ from this proof.

Introduction

The ultimate goal of radiation therapy (RT) is to eliminate tumor burden while sparing normal tissues from long-term injury. However current RT techniques expose both, normal tissues and tumors, to a wide range of dose size and fractionation, with a substantial amount of normal tissue being potentially irradiated (51). Herein the high intrinsic sensitivity of normal tissues to ionizing radiation (IR) often precludes the application of curative radiation doses (32,76). In particular thorax irradiation induces tissue inflammation (pneumonitis) and fibrosis within 12 weeks and 6-24 months after RT as dose-limiting side effects (12,22,37). The radiation-induced lung disease is a major obstacle to successful treatment of thorax-associated tumors (7,38). The pronounced radiosensitivity of the lung tissue is also dose-limiting when the whole body is irradiated prior to hematopoietic stem cell transplantation (24,40). Therefore current research efforts are aimed to develop pharmacological treatment strategies to protect the healthy lung tissue from the toxic effects of IR. However, no causal strategy for the prevention or treatment of radiation-induced late damage to the lungs is available so far (5,46).

Studies in animal models and patient samples show a complex response of the lung tissue to radiation with multiple interactions between resident cells (epithelial cells, fibroblasts, endothelial cells), extracellular matrix molecules and infiltrating immune cells (1,32,69). Among these populations the non-dividing cells, the microvascular endothelial compartment has clearly been shown to play a central role in radiation toxicity in healthy tissues (15,61).

Particularly microvessels are extremely sensitive to IR: Irradiation often results in a rupture of the capillaries, thrombosis and telangiectasia (27). In small-sized arteries (having a thin muscular wall and measuring up to 100mm in external diameter), IR causes a neointimal proliferation, thrombosis, fibrinoid necrosis and acute arthritis whereas larger blood vessels (ample lumen and thick muscular wall, > 500mm external diameter) seem to be less affected (27). Interestingly, endothelial cells (EC) of various organs differ in their sensitivity to IR: *In vitro* studies show, for example, that sinusoidal EC of the liver are highly radioresistant,

Mesenchymal stem cell therapy protects lungs from radiation-induced endothelial cell loss by restoring superoxide dismutase 1 expression (doi: 10.1089/ars.2016.6748)
This paper has been peer-reviewed and accepted for publication, but has yet to undergo copyediting and proof correction. The final published version may differ from this proof.

whereas microvascular EC of the skin are rather radiosensitive (62). Others and we showed in preclinical studies that radiation-induced normal tissue toxicity in the lung is closely linked to vascular EC damage and dysfunction of the blood air barrier (9,25,31,84). However, the underlying mechanisms of radiation-induced adverse late effects are still not well understood and no causative radioprotective treatment is available to date.

Stem cell therapy is a promising option for the prevention or treatment of radiation-induced normal tissue injury as it can promote survival and repair of damaged resident cells (14,42). However, there is a lack of preclinical and clinical studies of stem cell therapy for radiation-induced adverse effects in the lung, particularly in radiation-induced fibrosis (54,75). There are also only few ongoing clinical trials with mesenchymal stem cells (MSCs), also referred to as multipotent mesenchymal stromal cells (MPSCs) in chronic lung disease including their therapeutic application in patients with idiopathic pulmonary fibrosis (77). Importantly, beneficial or adverse effects of stem cell therapy on the pathogenic process seem to depend on the timing of stem cell application after radiotherapy. We previously demonstrated that therapeutic application of MSCs has the potential to counteract radiation-induced normal tissue damage when the MSC therapy is performed within 2 weeks after irradiation (44). We also showed that both, MSC derived classically from bone marrow (BM) or from aorta (vascular wall-derived MSCs) have the potential to protect lung EC from radiation-induced vascular leakage observed at 3 weeks post-irradiation as well as the associated increased extravasation of infiltrating immune cells and circulating tumor cells. Furthermore we demonstrated that vascular wall-derived MSCs are particularly well suited for the radioprotection of EC within the processes of radiation-induced lung injury because of their tissue-specific action (42,44). Thus, these findings greatly adhere to the concept of the low-toxicity multi-therapies presented recently in a position paper focusing on broad-spectrum approach cancer prevention and therapy (6). To further confirm that MSC therapy is able to downgrade the side effects of radiotherapy in a way that it could be called a low-toxicity approach in the future, we investigated the therapeutic potential of adoptive MSC transfer to

protect lung EC from radiation-induced damage, dysfunction and loss in the long-term follow-up and aimed at defining the mechanisms underlying the protective effects of MSC therapy.

Mesenchymal stem cell therapy protects lungs from radiation-induced endothelial cell loss by restoring superoxide dismutase 1 expression (doi: 10.1089/ars.2016.6748)
This paper has been peer-reviewed and accepted for publication, but has yet to undergo copyediting and proof correction. The final published version may differ from this proof.

Mesenchymal stem cell therapy protects lungs from radiation-induced endothelial cell loss by restoring superoxide dismutase 1 expression (doi: 10.1089/ars.2016.6748)
This paper has been peer-reviewed and accepted for publication, but has yet to undergo copyediting and proof correction. The final published version may differ from this proof.

Results

MSC treatment protects irradiated lung from severe radiation-induced vascular EC damage and delayed EC loss

In order to investigate the adverse late effects of radiation on the lung endothelium we performed intensive morphological analysis of lungs from mice (C57BL/6) at 25 weeks after WTI using electron microscopy (Figure 1). As expected, a massive collagen deposition in WTI lungs (15Gy) confirmed the development of lung fibrosis as a classical long-term complication of WTI (Figure 1A, B). Moreover, WTI induced multiple signs of severe morphological impairment in EC such as partially degraded mitochondria and numerous vacuoles as well as a defective and irregular basement membrane lining arterial EC (Figure 1C, D; Supplemental Figure S1) whereas no such alterations were observed in lung tissue of sham controls (0Gy) (Figure 1E, F). In contrast, a regular vessel structure as well as EC morphology was present in the lungs of MSC-treated animals which had received single cell suspensions of cultured MSCs ($0.5*10^6$ cells) derived from the aorta (Ao) or from the bone marrow (BM) within 24 hours after irradiation by intravenous injection (Figure 1G-L).

Next we were interested whether radiation-induced EC damage would result in an EC loss at late time points. Therefore we quantified the amount of vascular endothelial (VE)-cadherin, a protein specific to endothelial adherence junctions, in whole protein lysates by Western blot analysis (Figure 2A, B). In addition we quantified the number of EC in crude cell extracts of freshly isolated lung tissue using endothelial-specific PECAM1/CD31 expression and FACS analysis (Figure 2C). WTI induced a significant reduction of VE-Cad expression levels (mean 0Gy: 1.63±0.11, n=4; mean 15Gy: 0.61±0.04, n=4; 95% confidence interval of difference 0Gy vs. 15Gy: 0.68 to 1.37;) whereas in MSCs treated animals expression levels were partially restored (mean 15GyAo24h: 1.00±0.08, n=4; 95% CI of diff. 15Gy vs. 15GyAo24h: -0.74 to -0.05 and 95% CI of diff. 0Gy vs. 15GyAo24h: 0.28 to -0.97; mean 15GyBM24h: 0.76±0.04, n=4). Furthermore, flow cytometry analysis of the relative number of PECAM1/CD31 expressing cells further confirmed a significant EC loss at 25 weeks after WTI (0Gy:

Mesenchymal stem cell therapy protects lungs from radiation-induced endothelial cell loss by restoring superoxide dismutase 1 expression (doi: 10.1089/ars.2016.6748)
This paper has been peer-reviewed and accepted for publication, but has yet to undergo copyediting and proof correction. The final published version may differ from this proof.

35.73±1.62, n=4; 15Gy: 16.48±1.10, n=6; mean difference 0Gy vs. 15Gy: 19.2; 95% CI of diff. 13.7 to 24.8). Again the number of PECAM1/CD31 expressing cells were less reduced in animals which received a single MSC injection at 24h after irradiation (mean 15GyAo24h: 23.82±1.26, n=6; md 15Gy vs. 15GyAo24h: -7.33; 95% CI of diff. -12.3 to -2.38; and md 0Gy vs. 15GyAo24h: 11.9 95% CI of diff. 0Gy vs. 15GyAo24h: 6.37 to 17.4; mean 15GyBM24h: 20.53±1.07, n=4; md 15Gy vs. 15GyBM24h: -4.05; 95% CI of diff. -10.1 to 2.01). Immunohistochemistry (IHC) analysis of VE-Cad further revealed a less prominent staining of EC in lung sections of WTI mice which was restored in lung sections of WTI and subsequent MSC-treated animals (Figure 2D).

To further gain insight which vessel structures are affected by IR, smooth muscle cell (SMC)-stabilized vessels were quantified by counting the SMC marker-protein positive transgelin (Tagln)-immunoreactive vascular structures in whole tissue sections (Supplemental Figure S2). The amount of Tagln-positive vessels were significantly reduced at 25 weeks after WTI (mean 0Gy: 19.00±1.38, n= 8; mean 15Gy: 10.00±1.19, n=7; 95% CI of diff. 4.08 to 13,92) and were nearly normalized in animals which received a single AoMSC injection at 24h after irradiation and by tendency in animals which received BM-MSCs (mean 15GyAo24h: 16,60±0,68, n=5; 95% CI of diff. to 15Gy. -12.17 to –1.03; mean 15GyBM24h: 12.00±2.16, n=4; 95% CI of diff. to 15Gy: -7.96 to 3.96).

Interestingly, we also observed an increased number of total $CD45^+$ leukocytes in irradiated lungs at 25 weeks after WTI when compared to sham controls (Figure 2E, F). Particularly the percentage of potential profibrotic $CD11b^+$ myeloid cells and Ly6C monocytes (not shown) from $CD45^+$ leukocytes was significantly increased after WTI potentially as a direct consequence of impaired vascular function and EC loss (Figure 2F). Importantly, the radiation-induced increase in infiltration of these myeloid cells was significantly reduced in MSC-treated animals at 25 weeks after WTI which might be due to the protection of lung EC (Figure 2E, F).

Radiation-induced EC loss at 25 weeks after WTI was accompanied by the development of significant fibrosis as revealed by histological stainings on sections of paraffin-embedded

Mesenchymal stem cell therapy protects lungs from radiation-induced endothelial cell loss by restoring superoxide dismutase 1 expression (doi: 10.1089/ars.2016.6748)
This paper has been peer-reviewed and accepted for publication, but has yet to undergo copyediting and proof correction. The final published version may differ from this proof.

lung tissue with Masson´s Goldner Trichrome (Figure 3 A-C), Western blot analysis for significantly increased Collagen (Col1A1) expression levels of total lung lysates (Figure 3D, E), qRT-PCR quantifications of the extracellular matrix components Col1A2, Col3A1 and fibronectin 1 (Fn1) (Figure 3F), and IHC of the major extra cellular matrix glycosaminoglycan hyaluronan, respectively (Figure 3G). In all analyses, radiation-induced lung fibrosis was significantly attenuated by MSCs treatment (Fig. 3A-G).

Treatment of cultured lung microvascular EC with MSC-derived supernatants rescued radiation-induced endothelial damage

Up to now our data indicated that adoptive transfer of MSC provides long-term protection of lung EC from radiation-induced damage. To corroborate the assumed protective action of factors secreted from MSCs on EC we purified lung microvascular EC (LMEC) from *ex vivo* isolated crude lung cell extracts by PECAM1/CD31 antibody and immunomagnetic separation and compared cell viability and proliferation of irradiated LMEC cultured in normal growth medium, control supernatant or supernatants (SN) derived from cultured aortic MSCs and BM-MSCs (Figure 4A, B). Interestingly treatment with MSC supernatants rescued the radiation-induced reduction in viability and proliferation of LMEC. Interestingly, the protective effects of AoSN were more pronounced when compared to BMSN. LMEC migration using a wound closure assay and sprouting/invasion using ex vivo isolated lung explants embedded in growth factor-reduced matrigel were also significantly reduced on irradiation with different radiation doses; again treatment with AoSN rescued these effects more efficiently than treatment with BMSN (md 0Gy: ConSN vs. AoSN: -78.32; 95% CI of diff. -145.8 to -10.79 and md ConSN vs. BMSN: -6.69; 95% CI of diff. -74.18 to 60.87; md 15Gy: ConSN vs. AoSN: -251,4; 95% CI of diff. –247.0 to -111.9 and md ConSN vs. BMSN: -71.96; 95% CI of diff. -4.44 to 139.5) (Figure 4C, D). In line with these findings, a long-term assay measuring the surviving fraction after irradiation revealed that the number of LMEC able to regrow and form colonies after irradiation were significantly increased when cultured in the presence of MSC supernatants derived from cultured aortic or BM MSCs (md ConSN vs. AoSN: -0.0214;

Mesenchymal stem cell therapy protects lungs from radiation-induced endothelial cell loss by restoring superoxide dismutase 1 expression (doi: 10.1089/ars.2016.6748)
This paper has been peer-reviewed and accepted for publication, but has yet to undergo copyediting and proof correction. The final published version may differ from this proof.

95% CI of diff. -0.0267 to -0.0161 and md ConSN vs. BMSN: -0.0183; 95% CI of diff. -0.0237 to 0.013) (Figure 4E, F).

Therapeutically applied stem cells secrete superoxide dismutase 1 (SOD1) and restore SOD1 expression in WTI treated lungs

In order to identify MSC-secreted factors with radioprotective potential we compared supernatants from cultured aortic MSCs, BM MSCs or control supernatants by label free quantitative mass spectrometry (16). Among the list of identified protein groups our attention was attracted by SOD1 as this protein was identified in AoSN and BMSN supernatants but was below detection limit in control supernatants (Figure 5A; for complete list see Supplementary Table 1).

Western blot analysis of SOD1 expression levels confirmed the presence of SOD1 secreted from cultured MSCs in cell culture-derived supernatants (Figure 5B). SOD1 protein expression levels were further analyzed in whole protein lysates of control and WTI lungs with and without MSC treatment by Western blot analysis at 25 weeks post irradiation (Figure 5C, D). Of note, SOD1 expression levels were significantly reduced in lungs on WTI (mean 0Gy: 0.69±0.058, n=4; mean 15Gy: 0.40±0.14, n=4; md 0Gy vs. 15Gy: 0.285; 95% CI of diff. -0.119 to 0.689) and restored in lungs of irradiated animals that had received stem cell treatment (mean 15GyAo24h: 1.2±0.11, n=4; md 15Gy vs. 15GyAo24h: -0.699; 95% CI of diff. -1.103 to -0.295 and mean 15GyBM24h: 0.89±0.05, n=4; md 15Gy vs. 15GyBM24h: -0.498; 95% CI of diff. -0.902 to -0.009). IHC analysis of SOD1 expression corroborated a less prominent staining of EC in lung sections of WTI mice that was restored in lung sections of irradiated animals with MSC treatment (Figure 5E, Supplemental Figure S4).

Treatment with superoxide dismutase mimetic (EUK134) counteracts radiation-induced EC loss

To investigate whether restoration of SOD1 may contribute to the protective MSC action and counteract the RT-induced EC loss as adverse late effect we applied the superoxide

Mesenchymal stem cell therapy protects lungs from radiation-induced endothelial cell loss by restoring superoxide dismutase 1 expression (doi: 10.1089/ars.2016.6748)
This paper has been peer-reviewed and accepted for publication, but has yet to undergo copyediting and proof correction. The final published version may differ from this proof.

dismutase mimetic EUK134 during the first three weeks post-irradiation. Mice were sacrificed at 25 weeks post-irradiation and lung tissues were collected for further analysis. qRT-PCR quantification of SOD1 and also SOD2 as well as for the EC markers VE-Cad and VEGFR2/KDR demonstrated normalized expression levels of the genes in EUK134-treated animals as compared to a significant reduction after WTI (Figure 6A). To further determine restoration EC levels by EUK134 treatment we quantified the VE-Cad in whole protein lysates by Western blot analysis 25 weeks after irradiation (Figure 6B). WTI induced a significant reduction of VE-Cad expression levels (mean 0Gy: 0.71±0.06, n=6; mean 15Gy: 0.38±0.05, n=6; md 0Gy vs. 15Gy: 0.33; 95% CI of diff. 0.068 to 0.606) 25 weeks after irradiation whereas in EUK134-treated animals these expression levels were restored to the levels of sham controls (mean 15GyEUK: 0.64±0.08, n=7; md 15Gy vs. 15GyEUK: -0.263; 95% CI of diff. -0.523 to 0.127). Furthermore, while radiation-induced EC loss at 25 weeks after WTI was accompanied by a significant fibrosis progression RT-induced fibrosis was significantly reduced by an early treatment with the antioxidant EUK134 as revealed by Masson´s Goldner Trichrome staining (Figure 6C), as well as determination of the expression of the pro-fibrotic cytokine transforming growth factor-beta 1 (TGFb), respectively (Figure 6D).

Radiation of cultured tissue-resident MSCs results in decreased expression levels of SOD1 and induces a fibroblast-like phenotype

To investigate whether RT affects SOD1 expression of endogenous-lung resident MSCs, cultured MSCs derived from the aorta of Nestin-GFP (NestGFP)-transgenic mice were used as a model for tissue-resident MSCs. Phase contrast microscopy revealed morphological alterations of cultured AoMSCs after irradiation with 15Gy when a more enlarged and flattened fibroblast-like phenotype became prominent (Figure 7A). qRT-PCR analysis was performed to confirm the acquired fibroblast-like phenotype after irradiation. The fibroblast marker genes FAP for activated fibroblasts and transgelin (Tagln) for contractible fibroblasts (myo-fibroblasts) as well as genes encoding for extracellular matrix proteins (collagens and

Mesenchymal stem cell therapy protects lungs from radiation-induced endothelial cell loss by restoring superoxide dismutase 1 expression (doi: 10.1089/ars.2016.6748)
This paper has been peer-reviewed and accepted for publication, but has yet to undergo copyediting and proof correction. The final published version may differ from this proof.

fibronectin) were up-regulated after irradiation whereas SOD1 was significantly downregulated (Figure 7B). Western blot analysis for SOD1 protein expression levels revealed a downregulation of SOD1 in cell lysates as well of secreted SOD1 in cell culture supernatants of irradiated AoMSCs 96 hours after 15Gy irradiation as well as a significant down-regulation of the MSC-marker protein Nestin (Figure 7C). To further investigate the role of tissue-resident MSCs after WTI directly in the lungs, Nest-GFP mice were left untreated or received a 15Gy WTI. Histological evaluations confirmed the development of fibrosis 25 weeks after WTI as visualized by a massive collagen deposition (mean 0Gy: 2.78±0.29, n=6 vs. 15Gy: 5.12±0.25, n=15; $P \leq 0.001$) (Figure 7D), as well as a significant downregulation of SOD1 (Supplemental Figure S5). Lung sections were further stained for the activated fibroblast marker FAP and the MSC marker GFP which is under the regulatory control of the Nestin promotor (Figure 7D). FAP immunoreactivity confirmed the presence of activated fibroblasts in the fibrotic areas of WTI lungs and interestingly an increase of GFP expressing cells were also observed within this fibrotic areas whereas in not irradiated control lungs only singly GFP-positive MSCs could be detected (Figure 7D, arrow). Westernblot analysis of GFP expression in whole lung protein lysates confirmed a significant increase of NestGFP (Supplemental Figure S4).

Tissue-resident NestGFP(+) cells and not BM-derived MSCs contribute to fibrosis development

Next, we analyzed the putative contribution of tissue-resident lung MSCs as compared to BM-derived MSCs to fibrosis development. Therefore NestGFP transgenic mice were lethally irradiated with a split dose of 7+3 Gy TBI and subsequently adoptively transferred with BM cells from C57BL/6 donor mice into the tail vein (Nest wtBM) and vice-versa (wt NestBM). Un-irradiated NestGPF mice were used as control. Histological evaluations with Masson´s Goldner Trichrome on paraffin-embedded lung sections at 25 weeks after WTI confirmed fibrosis development in the lungs of TBI mice although the degree of fibrosis displayed a mild phenotype as revealed by the decreased Ashcroft scores as compared to WTI NestGFP

Mesenchymal stem cell therapy protects lungs from radiation-induced endothelial cell loss by restoring superoxide dismutase 1 expression (doi: 10.1089/ars.2016.6748)
This paper has been peer-reviewed and accepted for publication, but has yet to undergo copyediting and proof correction. The final published version may differ from this proof.

mice (mean 0Gy: 1.71±0.21, n=7 vs. 15Gy: 2.85±0.23, n=14; 95% CI of diff. -1.97 to -0.30) (Figure 8A). Significantly increased Tgfb1 and FAP protein expression by Western blot analysis in whole protein lung lysates further confirmed the fibrosis phenotype after TBI (Figure 8B). Interestingly, determination of GFP expression levels corroborated that lung-resident and not BM-derived GFP(+) MSCs contribute to fibrosis development as revealed by significantly increased GFP expression levels in Nest wtBM lungs (Figure 8C).

Mesenchymal stem cell therapy protects lungs from radiation-induced endothelial cell loss by restoring superoxide dismutase 1 expression (doi: 10.1089/ars.2016.6748)
This paper has been peer-reviewed and accepted for publication, but has yet to undergo copyediting and proof correction. The final published version may differ from this proof.

Discussion

Here we show for the first time that adoptive transfer of MSCs during the early phase after irradiation efficiently counteracts vascular damage and EC loss as adverse late effects of IR in a preclinical murine model of radiation-induced pneumopathy. Furthermore, MSC-derived cell culture supernatants efficiently rescued cultured lung EC from the radiation-induced toxic effects in short-term and long-term survival assays indicating the contribution of MSC-secreted factors. Finally, we identified MSC-derived SOD1 as potential paracrine mediator of the protective MSC action: i) MSCs secreted SOD1 into the culture SN; ii) therapeutically applied MSCs isolated either from the BM or the aorta have the potential to restore SOD1 expression in previously irradiated lung tissue when applied early after WTI; iii) irradiation of cultured AoMSCs as an *in vitro* model for endogenous lung MSCs led to a decrease in the expression and secretion of SOD1*;* iv) the protective effect of MSCs was mimicked by therapeutic application of the SOD-mimetic EUK134 and may involve besides protection of lung EC also the protection of endogenous lung-resident MSCs. These findings contribute to an improved understanding of radiation-induced normal tissue toxicity as main dose-limiting side effect of RT and can be of direct clinical relevance, since they suggest SOD1 as potential therapeutic target for the radioprotection of EC. Furthermore, the present data extend our earlier observations that therapeutically applied MSCs are well suited to protect lung EC from vascular dysfunction at early time-points post WTI and to limit associated immune cell infiltration in the previously irradiated lungs at the onset of the pneumonitic phase (44).

In more detail, we showed for the first time that adoptive transfer of MSC within the early phase after irradiation has the potential to provide a long-term protection of pulmonary EC from radiation-induced damage. It is generally accepted that blood vessels are critical components of the radiation response and that vascular damage upon irradiation is particularly prominent in the radiation response of normal tissues (9,25,31,44,84). We and

Mesenchymal stem cell therapy protects lungs from radiation-induced endothelial cell loss by restoring superoxide dismutase 1 expression (doi: 10.1089/ars.2016.6748)
This paper has been peer-reviewed and accepted for publication, but has yet to undergo copyediting and proof correction. The final published version may differ from this proof.

others showed that thorax irradiation results in impairment of various pulmonary vascular parameters such as structural changes in pulmonary blood vessels, vascular leakage, increased extravasation of circulating immune and tumor cells, as well as stenosis and lumen occlusion promoting increased pulmonary vascular resistance (25,29,34,44). In general the response of the vasculature to radiation is classified in acute and late effects, both of which contribute to the initiation, progression and maintenance of tissue damage (15). High doses of radiation (> 10Gy), can cause a rapid wave of EC apoptosis whereas surviving cells develop a dysfunctional vascular phenotype (57). Long-term effects include microvessel collapse, thickening of the basement membrane, and persistence of an activated, pro-coagulant endothelial phenotype (15,29). As a consequence the irradiated tissue is converted into a hypoxic, pro-inflammatory environment causing further damage to other normal cells by inducing ischemia, necrosis and fibrosis (15,74). The special importance of the primary injury to the EC for radiation-induced late toxicity in the lungs is emphasized by studies on pulmonary arterial hypertension where a functional impairment or even partial loss of the EC could be detected immediately after a selective lung irradiation and long before the manifestation of the first clinical symptoms (33). Here we show now that adoptive transfer of MSCs within the early phase after irradiation also provides long-term protection from radiation-induced EC damage, EC loss and immune cell infiltration that translates in protection from fibrosis development. Our findings support the assumption that adoptive transfer of adult MSCs may be a valuable therapeutic option for the prevention of lung diseases, the regeneration of diseased lung tissue or both because of their relatively easy availability, multipotent differentiation capacities, and immunomodulatory effects (4,77).

Importantly, in the present study aorta-derived MSCs were more potent than classically derived BM-MSC to protect lung EC from the adverse late effects of RT. These findings support our assumption that the high activity of the AoMSCs for EC protection might be due to the fact that tissue-specific stem cells mainly support the tissue type from which they originate (26,42,44). Within all our experiments concerning the EC (e.g. Western blot analysis, qRT-PCR and IHC for VE-Cad expression, CD31 FACS analysis, as well as

Mesenchymal stem cell therapy protects lungs from radiation-induced endothelial cell loss by restoring superoxide dismutase 1 expression (doi: 10.1089/ars.2016.6748)
This paper has been peer-reviewed and accepted for publication, but has yet to undergo copyediting and proof correction. The final published version may differ from this proof.

determination of Tagln-positive vessels) BM-MSCs did not appear to produce a robust improvement of the radiation-induced vascular damage, although BM-MSCs were able to limit fibrosis progression though not as effective as AoMSCs. Our data might suggest that BM-MSCs have a weaker response overall and in particular for the radioprotection of vascular EC. Affirmative, earlier reports already suggested that BM-MSC were less effective for MSC-therapy as compared to other stem cell sources, e.g. as compared to adipose tissue-derived or fetal MSCs (64,66,86).

Mechanistically, MSC-mediated protection was accompanied by restoration of normal expression levels of the antioxidant SOD1 in WTI lungs. Importantly, we identified SOD1 by a mass spectrometry approach as a paracrine factor that is secreted by aortic and BM-MSCs, but in particularly high amounts by AoMSCs. This corroborates the general view that engraftment in the lung is currently not considered the main mechanism by which MSCs repair a diseased lung tissue (36,78). Consistently we detected only a few, preferably single donor cells in WTI lung sections while circulating EGFP(+) MSCs could be detected in peripheral blood even 25 weeks after transplantation supporting the idea that tissue protection is due to paracrine signaling (44). Today it is widely accepted that the positive outcome of MSC therapy is not due to a direct engraftment of these cells into the lung e.g. as endothelial and epithelial cells, instead paracrine factors are now considered to be the main mechanism through which stem and progenitor cells exert their therapeutic effect (13). Herein it was suggested that MSCs may mediate their function through a ‘hit and run’ mechanism, where MSCs once temporarily loclized to the lung, may provide a local source of trophic factors in the pulmonary environment (8,13).

Our observation on the importance of up-regulation of the antioxidant enzyme SOD1 for MSC-mediated protection supports the current hypothesis that late pulmonary fibrosis develops from early damage to resident lung cells and that this early damage involves radiation-induced oxidative stress (29,48,80,87). Oxidative stress as a consequence of chemotherapy or radiotherapy or tissue inflammation promotes tissue damage including damage to the vasculature by activating a series of signaling pathways (47,65). Moreover,

Mesenchymal stem cell therapy protects lungs from radiation-induced endothelial cell loss by restoring superoxide dismutase 1 expression (doi: 10.1089/ars.2016.6748)
This paper has been peer-reviewed and accepted for publication, but has yet to undergo copyediting and proof correction. The final published version may differ from this proof.

accumulation of reactive oxygen species (ROS) causes cell apoptosis and necrosis, and can further contribute to myofibroblast activation (10,72). Consequently disease-promoting processes that are at least in part caused by oxidative damage can be targeted by increasing the antioxidant defense e.g. by the intake of, or supplementation with, antioxidants (19,28,59). Consistently, antioxidant treatment with the SOD mimetic EUK207 in the first month after thorax irradiation was able to protect against excessive collagen synthesis during the fibrotic stage (25-30 weeks) (29). The protective effect of EUK207 applied during the early phase after irradiation was associated with a partial mitigation of the radiation-induced vascular injury and reduction in blood vessel density observed as late effect of TBI of mice with 11 Gy (29), highlighting a role of oxidative stress for radiation-induced vascular injury. In line with these findings continuous administration of EUK-207 via implanted subcutaneous infusion pumps from 1 h until 14 weeks after irradiation also mitigated radiation-induced lung damage in rats (49). Even, when given after irradiation, a single injection of the SOD mimetic EUK-189 had a small but mitigating effect in rodents, especially in the lung (48). For some normal tissue radiation mitigation indications, a topical mean of delivering salen Mn complexes turned already been out to be therapeutically practical (68). Herein EUK-134 was reported as an effective combination catalase/SOD mimetic. In particular topical treatment with EUK-134 shortly before UVA exposure resulted in reduced levels of lipid peroxides at the surface of UVA-exposed skin but also baseline peroxide levels on non-irradiated skin were reduced in a dose-dependent fashion (20). As inhibition of H_2O_2 signaling using a EUK-134-like compound has already been shown to be a promising approach e.g. to breast cancer therapy it might also be possible that the protective effect of SOD1 and/or EUK-134 on counteracting radiation-induced EC loss could be mediated by H_2O_2 decomposition (71).

Our novel findings demonstrate for the first time that adoptive transfer of MSCs early after irradiation is also suited to enhance the antioxidant defense and to prevent radiation-induced late effects in irradiated WTI lungs by restoring expression levels of SOD1. MSC-mediated protection limited fibrosis progression presumably though secretion of SOD1. Notably, this protective effect of MSC therapy could be mimicked by the application of the SOD mimetic

Mesenchymal stem cell therapy protects lungs from radiation-induced endothelial cell loss by restoring superoxide dismutase 1 expression (doi: 10.1089/ars.2016.6748)
This paper has been peer-reviewed and accepted for publication, but has yet to undergo copyediting and proof correction. The final published version may differ from this proof.

EUK134: Application of EUK134 within the early phase after radiation counteracted EC loss and slightly but significantly reduced fibrosis development as long-term adverse effects of WTI. Furthermore, adoptive transfer of MSC also efficiently counteracted infiltration of immune cells at early (44) and at late stages as shown here. This is particularly important since oxidative stress generated by radiotherapy or chemotherapy is known to initiate a cascade of acute and chronic inflammatory reactions that may further increase oxidative stress in the inflamed tissue (3,30). Thus by addressing both, oxidative stress and tissue inflammation, MSC therapy may serve as an ideal mitigator of adverse late effects of radiotherapy. Herein mitigation refers to therapies that are started after irradiation but before there is overt evidence of clinical disease (29,58). Interestingly, MSC treatment particularly reduced the infiltration of profibrotic myeloid cells that had been shown to facilitate the progression of pulmonary fibrosis in the bleomycin-induced fibrosis model (35,63). The reduced infiltration of myeloid cells with an assumed profibrotic phenotype here after MSC therapy highlighted the importance of the proper function of the vascular system to avoid fibrosis development.

Interestingly, a normal function of resident MSCs in adult lungs is crucial for pulmonary tissue homeostasis as they contribute to the maintenance of tissue integrity by various mechanisms (39,53,55). As an example, endogenous lung MSCs normally exert anti-inflammatory properties; these are however negatively affected by bleomycin treatment thereby contributing to fibrosis development in a murine model of bleomycin-induced fibrosis (39). In line with these findings, exogenous administration of untreated lung MSCs protected lung integrity from bleomycin-induced lung injury and associated oxidative stress (39). Thus, in certain situations, external stimulation e.g. exogenously applied MSCs may be required to catalyze the repair suggesting an important role of transplanted cells to act as an initiator to trigger endogenous stem cell-based tissue repair (23).

In contrast, endogenous lung-resident MSCs were also shown to promote fibrotic remodeling by acquisition of a profibrotic myofibroblast phenotype e.g. upon stimulation with the pro-

Mesenchymal stem cell therapy protects lungs from radiation-induced endothelial cell loss by restoring superoxide dismutase 1 expression (doi: 10.1089/ars.2016.6748)
This paper has been peer-reviewed and accepted for publication, but has yet to undergo copyediting and proof correction. The final published version may differ from this proof.

fibrotic cytokine TGFb (52,73). Here we used cultured AoMSC as an *in vitro* model for endogenous lung MSCs and observed that radiation-induced the acquisition of a fibroblast-like phenotype that was associated with down-regulation of SOD1 expression and secretion. We are well aware of the fact that tissue-resident MSCs are heterogeneous and that different MSC subsets exist. The characterization and/or isolation of the stem cell subpopulations represent a major challenge to improve the efficacy of transplantation protocols used in regenerative medicine and applied to lung disorders (13). Primary lung MSCs which were enriched in the CD90/CD105 mononuclear cell fraction were shown to be located perivascularly (67). Therefore we think that vascular wall-derived MSCs used in our studies were a suitable model. We further used NestGFP transgenic mice in which endogenous Nestin-expressing MSCs where GFP-tagged to show that these lung-resident MSCs contribute to remodeling of lung tissue upon fibrosis development after WTI. Using BM-chimeras we further confirmed that indeed tissue-resident and not BM-derived MSCs were predominantly involved in fibrosis development. Interestingly increasing amounts of GFP were detected in fibrotic lungs of NestGFP mice after WTI and in Nest wtBM chimeras after TBI, although an induction of resident MSCs differentiation would firstly suggest a down-regulation of MSC marker proteins (namely Nestin) and thus of GFP. In line with our findings immunofluorescence microscopy already revealed that Nestin is expressed, in small proportions of fibroblasts (70). Furthermore a concomitant appearance of Nestin- and CD34-positive myofibroblasts was observed under fibrosing conditions suggesting that the differential expression of Nestin may not only indicate phenotypic and functional heterogeneity but also indicate that Nestin-positive myofibroblast may represent a relatively immature subpopulation of cells with multipotentiality (41).

These findings demonstrate that damage to tissue-resident lung MSCs may contribute to progression of radiation-induced fibrosis. However, we show for the first time that a reduced antioxidant capacity of MSC e.g. induced by the loss of SOD1 may be critical for development of a profibrotic MSC phenotype. In line with this assumption Chow et al. previously demonstrated that depletion of extracellular SOD in resident lung MSCs resulted

Mesenchymal stem cell therapy protects lungs from radiation-induced endothelial cell loss by restoring superoxide dismutase 1 expression (doi: 10.1089/ars.2016.6748)
This paper has been peer-reviewed and accepted for publication, but has yet to undergo copyediting and proof correction. The final published version may differ from this proof.

in microvascular remodeling and increasing muscularization in a murine model of pulmonary arterial hypertension (PAH) (11). Moreover, loss of SOD in cultured lung MSCs resulted in accelerated proliferation as well as increased multilineage differentiation potential and promoted the transition to a contractile phenotype (11) while suppression or elimination of excessive ROS turned out to be an effective strategy for improving the survival rate of transplanted MSC (85). Altogether these findings demonstrate that adoptive transfer of functional MSC has the potential to protect besides EC also the endogenous lung-resident MSCs from radiation-induced activation and subsequent differentiation into fibrosis-promoting fibroblast-like cells.

Conclusively our findings highlight the importance of radiation-induced damage to the vascular system within the processes of fibrosis progression (Figure 9). While the exact mechanisms by which therapeutically applied MSCs as well as the SOD-mimetic EU134 prevent vascular cell loss is not known, its ability to reduce radiation-induced apoptosis in capillary EC cultures may be relevant as it results in improved clonogenic EC survival as shown here and by others (21,79). In addition to a direct protective effect on the lung endothelium, proper vascular function and restoration of SOD1 expression may contribute to a microenvironment, e.g. through normalization of immune cell infiltration, that favors both prevention of, and recovery from, radiation injury to vascular and other resident lung cells. In support of this hypothesis we show here that elevated SOD1 expression levels after treatment protect resident MSCs presumably by inhibiting differentiation into a fibroblast-like phenotype. However, further studies are needed to clarify the mechanistic link between effects on ECs and lung-resident MSCs and damage of other lung parenchymal cells e.g. alveolar or bronchial epithelial cells for fibrosis development. MSC treatment could also antagonize radiation-induced senescence of bronchial-alveolar epithelial cells and thus prevent up-regulation of the senescence-associated secretory phenotype (SASP) factors and subsequent recruitment of inflammatory myeloid cells as late adverse effects which was already shown for to be blocked early after radiation (44). Further investigations will also be performed in the future to corroborate our findings in more clinical relevant settings such as

fractionated low-dose irradiation. Understanding the mechanisms and in particular the advantage of AoMSC-mediated protection of EC cells from the adverse effects of IR is required to if we want to develop MSC-based protective treatment strategies.

Innovation (100 words)

Current research efforts are aimed to develop treatment strategies to protect the healthy lung tissue from toxic effects of ionizing radiation. In this study we highlight the structures of lung endothelia as key players in the progression of radiation-induced lung disease and in particular EC loss as long-term complication after radiation conveys the development of fibrosis. Adoptive transfer of MSCs in the early phase after irradiation limits the radiation-induced EC loss and fibrosis progression by restoration of the antioxidant enzyme SOD1. Thus, adoptive transfer of MSCs early after irradiation is a promising strategy to radioprotect lungs from radiation-induced late damage.

Mesenchymal stem cell therapy protects lungs from radiation-induced endothelial cell loss by restoring superoxide dismutase 1 expression (doi: 10.1089/ars.2016.6748)
This paper has been peer-reviewed and accepted for publication, but has yet to undergo copyediting and proof correction. The final published version may differ from this proof.

Methods

Whole thorax irradiation (WTI) mouse model

Wild type C57BL/6 and Nestin-GFP (NestGFP) transgenic donor mice (mixed gender) received 15 Gray of WTI in a single dose of a Cobalt 60 source (^{60}Co γ-rays at 0.5 Gy/min) as previously described (43,44,81). Single cell suspensions of cultured MSCs ($0.5*10^6$ cells) were intravenously transplanted into the tail vein of WTI mice 24 hours or 14 days after irradiation or in sham irradiated (0Gy) control animals as previously described (44). All procedures involving mice were approved by the local institutional Animal Care Committee (Regierungspräsidium Düsseldorf Az84-02.04.2012.A137; 84-02.04.2012.A034). For mimicking MSC action (restoring SOD1 expression) a synthetic superoxide dismutase mimetic (EUK134, from Selleckchem, Houston, TX) was used. Within combined treatment, WT mice were exposed to WTI and subsequently treated three times a week (starting within 24 hours after WTI) within the first three weeks post-irradiation by intraperitoneal injection with 100 µl solvent (PBS) or 10 µg/g bodyweight EUK134 (diluted in 100µl PBS). Mice were sacrificed at 25-30 weeks post-irradiation and lung tissues were collected for further analysis.

Total body irradiation (TBI) mouse model

A mouse TBI model was used as described before (43,44). In brief, BM cells were harvested aseptically by flushing the tibias and femurs of adult animals and subjected to erythrocytes lysis. C57Bl/6J (both gender) mice were lethally irradiated with a split dose (7+3 Gy) of a X-ray source and were intravenously transplanted with $1x10^6$ unfractionated murine NestGFP-expressing BM cells from Nestin-GFP transgenic donor mice into the tail vein (wt NestBM) (83). After 25 weeks animals were sacrificed and lungs were isolated. In addition, a vice versa experiment was performed: NestGFP mice were lethally irradiated and BM cells from C57Bl/6 wild type donor mice were transplanted (Nest wtBM). Experiments were repeated three times.

Mesenchymal stem cell therapy protects lungs from radiation-induced endothelial cell loss by restoring superoxide dismutase 1 expression (doi: 10.1089/ars.2016.6748)
This paper has been peer-reviewed and accepted for publication, but has yet to undergo copyediting and proof correction. The final published version may differ from this proof.

Isolation and purification of aortic MSCs and bone marrow MSCs

Vascular wall resident MSC were isolated from aortas of C57BL/6-Tg(CAG-EGFP)1Osb/J mice (Jackson Laboratory, Bar Habor, ME) as previously described (43,44). In brief, tissue pieces were mechanically minced and dissociated for 15 minutes at 37°C in OptiMEM I medium containing 0.2% type 2-collagenase (CLS2, 43J14367B; Worthington, Lakewood, WA). Pure MSCs were generated using a Sca-1 antibody (130-092-529) and MACS technology (Miltenyi Biotec, Bergisch Gladbach, Germany) according to the manufacturer's instructions. Primary MSCs were cultivated on plastic plates in DMEM/20% FCS. Primary cultures were clonally expanded under limiting dilution conditions. BM cells were harvested and cultured using complete DMEM/ 20% FCS as previously described (44).

LMEC isolation

Lung microvascular EC (LMEC) were purified from type 2 collagenase digested cell extracts using the same MACS technology protocol in combination with biotinylated PECAM1 antibody (CD31 MEC 13.3, BD Bioscience, Franklin Lakes, NJ) and Streptavidin Microbeads. Cells were cultured in ECG medium MV (PromoCell, Heidelberg, Germany).

Real-Time reverse transcription PCR (qRT-PCR)

RNA was isolated using RNeasy Mini Kit (74106, Qiagen, Hilden, Germany) according to the manufacturer’s instruction and as previously described (44). Expression levels were normalized to the reference gene (beta actin; set as 1) and are shown as relative quantification. Specific primers were designed with the program Primer 3 (http://frodo.wi.mit.edu/cgi-bin/primer3/primer3_www.cgi) based on available NCBI nucleotide CDS sequences. Cross-reaction of primers was excluded by comparison of the sequence of interest with the NCBI database (Blast 2.2, U.S. National Centre for Biotechnology Information, Bethesda, MD) and all primers used in our study were intron-spanning. PCR products are 200-300 bp in size. qRT-PCR was carried out using specific oligonucleotide

Mesenchymal stem cell therapy protects lungs from radiation-induced endothelial cell loss by restoring superoxide dismutase 1 expression (doi: 10.1089/ars.2016.6748)
This paper has been peer-reviewed and accepted for publication, but has yet to undergo copyediting and proof correction. The final published version may differ from this proof.

primers (bActin_fw CCAGAGCAAGAGAGGTATCC, bActin_bw CTGTGGTGGTGAAGCTGTAG; Fn1_fw GAAACCTGCTTCAGTGTGTCTG, Fn1_bw TTGAATTGCCACCATAAGTCTG; Nestin_fw CCAAGAATGGAGGATCAAGAA, Nestin_bw TGGGTATTGGCTCTCCTCTTTA; GFP_fw GACGGGAACTACAAGACACG, GFP_bw CGAAAGGGCAGATTGTGTGG; VE-Cad_fw CAG CAC TTC AGG CAA AAA CA, VE-Cad_bw ATTCGGAAGAATTGGCCTCT; Col3A1_fw GATCCCATTTGGAGAATGTTGT, Col3A1_bw GATCCAGGATGTCCAGAAGAAC) as previously described (44).

Conditioned Media

Aortic MSCs and BM-MSCs were cultured in normal growth media until confluence. Media was replaced and cells were cultured in the presence of 0.5% fetal bovine serum for 24 hours before collection of media. Control media was generated by incubating the same medium (containing 0.5% fetal bovine serum) without cells. Conditioned media were used as 1/1 mixture with normal growth medium. For mass spectrometry analysis confluent cells were incubated for 48 hours with serum free media.

Sample preparation for liquid chromatography–mass spectrometry (LC-MS)

Proteins were precipitated with acetone (-20°C, overnight) and then resuspended in 50 mM phosphate buffer (pH 7.5). The protein concentration was determined using the Roti Nanoquant (Roth) protein assay. A volume corresponding to 15 µg total proteome was then transferred to a fresh Eppendorf tube and reduced (10 mM DTT, 45 min) and alkylated (20 mM iodoacetamide IAM, 60 min) at 37°C in the presence of 6M Urea. Afterwards the sample was incubated with LysC (ratio 1:50) at 37°C for 3h. Next the urea concentration was reduced to 1.8 M urea by addition of 50 mM ammonium bicarbonate (ABC) buffer. Subsequently trypsin was added (ratio 1:30) and the samples were incubated over night at 37°C while vigorously shaking. The digestion reaction was stopped by adding formic acid (final concentration 1%). The tryptic digests were desalted on home-made C18 StageTips.

Mesenchymal stem cell therapy protects lungs from radiation-induced endothelial cell loss by restoring superoxide dismutase 1 expression (doi: 10.1089/ars.2016.6748)
This paper has been peer-reviewed and accepted for publication, but has yet to undergo copyediting and proof correction. The final published version may differ from this proof.

After elution from the StageTips samples were dried using a vacuum concentrator and the peptides taken up in 15 µL 0.1 % formic acid solution.

LC-MS/MS

Experiments were performed on an Orbitrap Elite instrument (Thermo Fisher Scientific, Waltham, MA) that was coupled to an EASY-nLC 1000 liquid chromatography (LC) system (56). The LC was operated in the two-column mode. The home-made fused silica column equipped with a glass fiber frit was packed with Reprosil-Pur 120 C18-AQ 3 µm resin and connected to the analytical column via an UHPLC union (50). The analytical column was a fused silica capillary (75 µm × 25 cm) with integrated PicoFrit emitter packed in-house with Reprosil-Pur 120 C18-AQ 3 µm resin. The analytical column was attached to a nanospray flex ion source (Thermo Fisher Scientific). Peptides were delivered to the pre-column via the integrated autosampler at a flow rate of 2–3 µl/min in 100% solvent A (0.1% formic acid, FA, in UPLC grade water). Peptides were subsequently separated on the analytical column by running a 70 min gradient of solvent A and solvent B (start with 7% B; gradient 7% to 35% B (0.1% FA in acetonitrile, ACN) for 60 min; gradient 35% to 100% B for 5 min and 100% B for 5 min) at a flow rate of 300 nl/min.

The mass spectrometer (positive ion mode) was operated using Xcalibur software (version 2.2 SP1.48). Precursor ion scanning was performed in the Orbitrap analyzer (FTMS) in the scan range of m/z 300-1,500 and at a resolution of 120,000 with the internal lock mass option turned on (lock mass was 445.120025 m/z, polysiloxane)(60). Product ion spectra were recorded in a data dependent fashion in the ion trap (ITMS) in a variable scan range and at a rapid scan rate. The ionization potential (spray voltage) was set to 1.6 – 2.0 kV. Peptides were analyzed using a repeating cycle consisting of a full precursor ion scan (1.0 × 10^6 ions) followed by 15 product ion scans (1.0 × 10^4 ions) where peptides are isolated based on their intensity in the full survey scan (threshold of 500 counts) for tandem mass spectrum (MS2) generation that permits peptide sequencing and identification. CID collision energy was set to 35% for the generation of MS2 spectra. During MS2 data acquisition

Mesenchymal stem cell therapy protects lungs from radiation-induced endothelial cell loss by restoring superoxide dismutase 1 expression (doi: 10.1089/ars.2016.6748)
This paper has been peer-reviewed and accepted for publication, but has yet to undergo copyediting and proof correction. The final published version may differ from this proof.

dynamic ion exclusion was set to 120 seconds with a maximum list of excluded ions consisting of 500 members and a repeat count of one. Only charge states bigger than 1 were considered for fragmentation.

Label free quantification using MaxQuant

RAW spectra were submitted to an Andromeda (18) search in MaxQuant (version 1.5.0.25) using the default settings (17). Label-free quantification and match-between-runs was activated (16). MS2 spectra data were searched against a Uniprot mouse reference databse (MOUSE.fasta; 59375 sequences). All searches included a contaminants database (as implemented in MaxQuant, 263 sequences). The contaminants database contains known MS contaminants and was included to estimate the level of contamination. Andromeda searches allowed for oxidation of methionine residues (16 Da) and a static modification on cysteine (57 Da, alkylation with iodoacetamide). Enzyme specificity was set to Trypsin/P. For the Andromeda searches the default MaxQuant settings were used. Briefly, the precursor peptide tolerance for the first search was 20 ppm and for the main search 4.5 ppm. The ion trap MS/MS match tolerance was 0.5 Da. Label-free quantification and match-between-runs was switched on.

Flow cytometry analysis

Crude cell extracts of freshly isolated lungs were generated and FACS analysis was performed as previously described (44,81). Lung cell suspensions were stained with anti-mouse CD45 (30-F11; Cat. 103126 from BioLegend, San Diego, CA) to exclude leukocytes. Lung cells were further fluorochrome-labeled with anti-mouse CD31 (390; Cat. 11-0311, from eBioscience Frankfurt, Germany) and anti-mouse CD11b (M1/70, Cat. 101227 from BioLegend, San Diego, CA). Flow cytometric measurements were performed on a BD LSRII flow cytometer using FACS DIVA software. Analyses of obtained data sets were done using FACS DIVA software (all from BD Bioscience, Franklin Lakes, NJ).

Mesenchymal stem cell therapy protects lungs from radiation-induced endothelial cell loss by restoring superoxide dismutase 1 expression (doi: 10.1089/ars.2016.6748)
This paper has been peer-reviewed and accepted for publication, but has yet to undergo copyediting and proof correction. The final published version may differ from this proof.

Lung sprouting assay

Ex vivo isolated lung pieces were seeded on growth factor-reduced Matrigel in NGM supplemented with or without MSCs conditioned medium. Capillary-like outgrowth was quantified by measuring the sprouting distance 4 days post irradiation.

Western blot

Whole cell lysates were generated by scraping cells into ice-cold RIPA-P buffer (150 mmol/L NaCl, 1% NP40, 0.5% sodium-desoxycholate, 0.1% sodium-dodecylsulfate, 50 mmol/L Tris/HCL pH8, 10 mmol/L sodium fluoride (NaF), 1 mmol/L sodium orthovandanate (Na_3VO_4) supplemented with complete Protease-Inhibitor-Cocktail (04693159001, Hoffmann-La Roche, Basel, Switzerland) and performing 2–3 freeze-thaw cycles. Protein samples (50–100 µg total protein) were subjected to SDS-PAGE electrophoresis and Western blots were done as previously described using indicated antibodies (18,60). SOD1 (FL-154, sc22760), p21 (F8, sc271610), Col1A1 (D13, sc-25974), Nestin (10c2, sc-23927) and VE-Cad (C19, sc6458) antibodies were from Santa Cruz (Santa Cruz, CA), FAP (PA5-51057) and GFP (A-11122) antibodies were from Thermo Scientific (Dreieich, Germany), beta-actin (clone AC-74, A2228) antibody was from Sigma-Aldrich (St. Louis, MO).

Immunohistochemistry and electron microscopy

Paraffin-embedded tissue sections were hydrated using a descending alcohol series, incubated for 10–20 min in target retrieval solution (DAKO, Glostrup, Denmark) and incubated with blocking solution (2% FCS/PBS). After permeabilisation, sections were incubated over night at 4°C with primary antibodies (SOD1, VE Cad, Nestin, GFP each 1/100). Antigen was detected with a horseradish peroxidase-conjugated secondary antibody (1/250) and DAB staining (DAKO, Glostrup, Denmark). Nuclei were counterstained using hematoxylin. Electron microscopy was done as previously described (44).

Lung histopathology

Mesenchymal stem cell therapy protects lungs from radiation-induced endothelial cell loss by restoring superoxide dismutase 1 expression (doi: 10.1089/ars.2016.6748)
This paper has been peer-reviewed and accepted for publication, but has yet to undergo copyediting and proof correction. The final published version may differ from this proof.

For lung histology mice were narcotized using isoflurane (2-chloro-2-(difluoromethoxy)-1,1,1-trifluoro-ethane) and killed by transcardial perfusion with PBS. Whole inflation fixed lungs were taken out and lung tissue was fixed in 4% formalin and embedded in paraffin. Three to four 5-µm paraffin longitudinal cross-sections were taken per mouse lung at the midpoint through the lung block depth. Sections were stained with hematoxylin and eosin or Masson´s Goldner Trichrome (MT) (Carl Roth Karlsruhe, Germany) for histological evaluation. Samples were then analyzed microscopically with a 20× objective. Sections were scored blinded to the genotype and treatment group. In whole sections of lung parenchyma lung fibrosis from each specimen were scored using a 0 to 8 point Ashcroft scale (2,82). The mean scores (five per section) were averaged to yield the final score for each specimen. Depicted data represent the mean values of all mice per group (mean of single average number for each mouse/ mouse number) as indicated.

Irradiation of cell cultures

Radiation with indicated doses was performed using the Isovolt-320-X-ray machine (Seifert-Pantak, East Haven, CT, USA) at 320 kV, 10 mA with a 1.65-mm aluminum filter and a distance of about 500 mm to the object being irradiated. The effective photon energy was about 90 kV and the dose rate about 3 Gy/min.

Colony formation assay

For this long-term assay, 200–1600 cells/well were plated in six-well plates as previously described (45). After radiation with indicated doses plates were incubated for a total of 10 days to allow growth of single colonies. Cells were then fixed in 3.7% formaldehyde and 70% ethanol and subsequently stained with 0.05% Coomassie Brilliant Blue. Colonies (⩾50 cells/colony) were counted under the microscope at fivefold magnification. The survival curves were established by plotting the log of the surviving fraction against the treatment dose

Mesenchymal stem cell therapy protects lungs from radiation-induced endothelial cell loss by restoring superoxide dismutase 1 expression (doi: 10.1089/ars.2016.6748)
This paper has been peer-reviewed and accepted for publication, but has yet to undergo copyediting and proof correction. The final published version may differ from this proof.

Cell proliferation

After indicated time points and treatments cells were fixed with methanol for 10 min and stained with 0.5% crystal violet dye (in methanol: deionized water, 1:5) for 10 min. Excess crystal violet dye was removed by five washes of deionized water on a shaker (10 min for each wash) and the culture plates were dried overnight. The crystal violet dye was released from cells by incubation with 1% sodium dodecyl sulfate (SDS) for 1-2 hours before optical density (OD 595 nm) measurement. The cell proliferation reagent WST-1 was used as a ready-to-use colorimetric assay for the nonradioactive quantification of cellular, viability and cytotoxicity according to the manufactures instructions. Optical density (OD 450 nm) measurements were performed 60-90 min after incubation.

Migration assay

Migration of the cells was investigated via time lapse microscopy for 8 hours after IR. Therefore cells were grown to confluence, irradiated and a thin wound was introduced by scratching with a 10µl pipette tip. Wound closure was determined for the different treatments by measuring the migration distance using ImageJ 1.47t (Wayne Rasband, National Institutes of Health, US states).

Statistical analysis

If not otherwise indicated, data were obtained from 3 independent experiments with at least 3 mice each. Mean values were calculated and used for analysis of standard error (SEM) as indicated by error bars. Statistical significance was evaluated by 1-way ANOVA followed by Tukey's or Bonferroni multiple comparisons post-test. Statistical significance was set at the level of $P \leq 0.05$. Data analysis was performed with Prism 5.0 software (GraphPad, La Jolla, California).

Mesenchymal stem cell therapy protects lungs from radiation-induced endothelial cell loss by restoring superoxide dismutase 1 expression (doi: 10.1089/ars.2016.6748)
This paper has been peer-reviewed and accepted for publication, but has yet to undergo copyediting and proof correction. The final published version may differ from this proof.

Acknowledgements

We thank L. Lüdemann and M. Groneberg for support with the irradiation of mice, Holger Jastrow for the help in ultrastructural analysis, Mohamed Benchellal, Inge Spratte and Eva Gau for their excellent technical assistance. The work was supported by grants of the DFG (GRK1739/1; JE275/1; INST 20876/127-1 FUGG M.K.) the BMBF (ZISS 02NUK024-D), an ERC starting grant (M.K. 258413), and the UK Essen/IFORES (D/107-81040). Contributions: D.K., J.S., A.W., K.R., F.S. and F.K. performed experiments, D.K. supervised and analysed results and made the figures; M.K., J.F., M.Y. and M.S. provided materials; D.K. and V.J. designed research and wrote the paper. All authors read and approved the manuscript.

Author Disclosure Statement

The authors state that there are no personal or institutional conflicts of interest.

Mesenchymal stem cell therapy protects lungs from radiation-induced endothelial cell loss by restoring superoxide dismutase 1 expression (doi: 10.1089/ars.2016.6748)
This paper has been peer-reviewed and accepted for publication, but has yet to undergo copyediting and proof correction. The final published version may differ from this proof.

List of Abbreviations

Ao	aorta
BM	bone marrow
Ccl2	chemokine (C-C motif) ligand 2
CI	confidence intervall
DMEM	Dulbecco's Modified Eagle's Medium
DAB	3,3'-Diaminobenzidine
EC	endothelial cell
EGFP	enhanced green fluorescent protein
FCS	fetal calf serum
Gy	Gray
IR	ionizing radiation
IHC	immunohistochemistry
LMEC	lung microvascular EC (mouse)
md	mean difference
MPSC	multipotent stem cell/ multipotent stromal cells of mesenchymal nature
MSC	mesenchymal stem cell
PBS	phosphate buffered saline
RT	radiotherapy
RT-PCR	reverse transcription polymerase chain reaction
SD	standard deviation
SEM	standard error of the mean
SMC	smooth muscle cell
SN	supernatant
SOD1	superoxide dismutase 1
TBI	total body irradiation
VE-Cad	vascular endothelial cadherin
WTI	whole thorax irradiation

Mesenchymal stem cell therapy protects lungs from radiation-induced endothelial cell loss by restoring superoxide dismutase 1 expression (doi: 10.1089/ars.2016.6748)
This paper has been peer-reviewed and accepted for publication, but has yet to undergo copyediting and proof correction. The final published version may differ from this proof.

References

1. Almeida C, Nagarajan D, Tian J, Leal SW, Wheeler K, Munley M, Blackstock W, Zhao W. The role of alveolar epithelium in radiation-induced lung injury. *PLoS One* 8: e53628, 2013.
2. Ashcroft T, Simpson JM, Timbrell V. Simple method of estimating severity of pulmonary fibrosis on a numerical scale. *J Clin Pathol* 41: 467-70, 1988.
3. Azzam EI, Jay-Gerin JP, Pain D. Ionizing radiation-induced metabolic oxidative stress and prolonged cell injury. *Cancer Lett* 327: 48-60, 2012.
4. Benderitter M, Caviggioli F, Chapel A, Coppes RP, Guha C, Klinger M, Malard O, Stewart F, Tamarat R, Luijk PV, Limoli CL. Stem cell therapies for the treatment of radiation-induced normal tissue side effects. *Antioxid Redox Signal* 21: 338-55, 2014.
5. Bentzen SM. Preventing or reducing late side effects of radiation therapy: radiobiology meets molecular pathology. *Nat Rev Cancer* 6: 702-13, 2006.
6. Block KI, Gyllenhaal C, Lowe L, Amedei A, Amin AR, Amin A, Aquilano K, Arbiser J, Arreola A, Arzumanyan A, Ashraf SS, Azmi AS, Benencia F, Bhakta D, Bilsland A, Bishayee A, Blain SW, Block PB, Boosani CS, Carey TE, Carnero A, Carotenuto M, Casey SC, Chakrabarti M, Chaturvedi R, Chen GZ, Chen H, Chen S, Chen YC, Choi BK, Ciriolo MR, Coley HM, Collins AR, Connell M, Crawford S, Curran CS, Dabrosin C, Damia G, Dasgupta S, DeBerardinis RJ, Decker WK, Dhawan P, Diehl AM, Dong JT, Dou QP, Drew JE, Elkord E, El-Rayes B, Feitelson MA, Felsher DW, Ferguson LR, Fimognari C, Firestone GL, Frezza C, Fujii H, Fuster MM, Generali D, Georgakilas AG, Gieseler F, Gilbertson M, Green MF, Grue B, Guha G, Halicka D, Helferich WG, Heneberg P, Hentosh P, Hirschey MD, Hofseth LJ, Holcombe RF, Honoki K, Hsu HY, Huang GS, Jensen LD, Jiang WG, Jones LW, Karpowicz PA, Keith WN, Kerkar SP, Khan GN, Khatami M, Ko YH, Kucuk O, Kulathinal RJ, Kumar NB, Kwon BS, Le A, Lea MA, Lee HY, Lichtor T, Lin LT, Locasale JW, Lokeshwar BL, Longo VD, Lyssiotis CA, MacKenzie KL, Malhotra M, Marino M, Martinez-Chantar ML, Matheu A, Maxwell C, McDonnell E, Meeker AK, Mehrmohamadi M, Mehta K, Michelotti GA, Mohammad RM, Mohammed SI, Morre DJ, Muralidhar V, Muqbil I, Murphy MP, Nagaraju GP, Nahta R, Niccolai E, Nowsheen S, Panis C, Pantano F, Parslow VR, Pawelec G, Pedersen PL, Poore B, Poudyal D, Prakash S, Prince M, Raffaghello L, Rathmell JC, Rathmell WK, Ray SK, Reichrath J, Rezazadeh S, Ribatti D, Ricciardiello L, Robey RB, Rodier F, Rupasinghe HP, Russo GL, Ryan EP, Samadi AK, Sanchez-Garcia I, Sanders AJ, Santini D, Sarkar M, Sasada T, Saxena NK, Shackelford RE, Shantha Kumara HM, Sharma D, Shin DM, Sidransky D, Siegelin MD, Signori E, Singh N, Sivanand S, Sliva D, Smythe C, Spagnuolo C, Stafforini DM, Stagg J, Subbarayan PR, Sundin T, Talib WH, Thompson SK, Tran PT, Ungefroren H, Vander Heiden MG, Venkateswaran V, Vinay DS, Vlachostergios PJ, Wang Z, Wellen KE, Whelan RL, Yang ES, Yang H, Yang X, Yaswen P, Yedjou C, Yin X, Zhu J, Zollo M. Designing a broad-spectrum integrative approach for cancer prevention and treatment. *Semin Cancer Biol* 35 Suppl: S276-304, 2015.
7. Borst GR, Ishikawa M, Nijkamp J, Hauptmann M, Shirato H, Onimaru R, van den Heuvel MM, Belderbos J, Lebesque JV, Sonke JJ. Radiation pneumonitis in patients treated for malignant pulmonary lesions with hypofractionated radiation therapy. *Radiother Oncol* 91: 307-13, 2009.
8. Caplan AI, Dennis JE. Mesenchymal stem cells as trophic mediators. *J Cell Biochem* 98: 1076-84, 2006.
9. Cappuccini F, Eldh T, Bruder D, Gereke M, Jastrow H, Schulze-Osthoff K, Fischer U, Kohler D, Stuschke M, Jendrossek V. New insights into the molecular pathology of radiation-induced pneumopathy. *Radiother Oncol* 101: 86-92, 2011.
10. Chen C, Yang S, Zhang M, Zhang Z, Hong J, Han D, Ma J, Zhang SB, Okunieff P, Zhang L. Triptolide mitigates radiation-induced pulmonary fibrosis via inhibition of axis of alveolar macrophages-NOXes-ROS-myofibroblasts. *Cancer Biol Ther*: 1-9, 2016.
11. Chow K, Fessel JP, Kaoriihida S, Schmidt EP, Gaskill C, Alvarez D, Graham B, Harrison DG, Wagner DH, Jr., Nozik-Grayck E, West JD, Klemm DJ, Majka SM. Dysfunctional resident lung mesenchymal stem cells contribute to pulmonary microvascular remodeling. *Pulm Circ* 3: 31-49, 2013.
12. Coggle JE, Lambert BE, Moores SR. Radiation effects in the lung. *Environ Health Perspect* 70: 261-91, 1986.
13. Conese M, Carbone A, Castellani S, Di Gioia S. Paracrine effects and heterogeneity of marrow-derived stem/progenitor cells: relevance for the treatment of respiratory diseases. *Cells Tissues Organs* 197: 445-73, 2013.

Mesenchymal stem cell therapy protects lungs from radiation-induced endothelial cell loss by restoring superoxide dismutase 1 expression (doi: 10.1089/ars.2016.6748)
This paper has been peer-reviewed and accepted for publication, but has yet to undergo copyediting and proof correction. The final published version may differ from this proof.

14. Coppes RP, van der Goot A, Lombaert IM. Stem cell therapy to reduce radiation-induced normal tissue damage. *Semin Radiat Oncol* 19: 112-21, 2009.
15. Corre I, Guillonneau M, Paris F. Membrane signaling induced by high doses of ionizing radiation in the endothelial compartment. Relevance in radiation toxicity. *Int J Mol Sci* 14: 22678-96, 2013.
16. Cox J, Hein MY, Luber CA, Paron I, Nagaraj N, Mann M. Accurate proteome-wide label-free quantification by delayed normalization and maximal peptide ratio extraction, termed MaxLFQ. *Mol Cell Proteomics* 13: 2513-26, 2014.
17. Cox J, Mann M. MaxQuant enables high peptide identification rates, individualized p.p.b.-range mass accuracies and proteome-wide protein quantification. *Nat Biotechnol* 26: 1367-72, 2008.
18. Cox J, Neuhauser N, Michalski A, Scheltema RA, Olsen JV, Mann M. Andromeda: a peptide search engine integrated into the MaxQuant environment. *J Proteome Res* 10: 1794-805, 2011.
19. Day BJ. Antioxidants as potential therapeutics for lung fibrosis. *Antioxid Redox Signal* 10: 355-70, 2008.
20. Declercq L, Sente I, Hellemans L, Corstjens H, Maes D. Use of the synthetic superoxide dismutase/catalase mimetic EUK-134 to compensate for seasonal antioxidant deficiency by reducing pre-existing lipid peroxides at the human skin surface. *Int J Cosmet Sci* 26: 255-63, 2004.
21. Dimmeler S, Hermann C, Galle J, Zeiher AM. Upregulation of superoxide dismutase and nitric oxide synthase mediates the apoptosis-suppressive effects of shear stress on endothelial cells. *Arterioscler Thromb Vasc Biol* 19: 656-64, 1999.
22. Ding NH, Li JJ, Sun LQ. Molecular mechanisms and treatment of radiation-induced lung fibrosis. *Curr Drug Targets* 14: 1347-56, 2013.
23. Dong F, Caplan AI. Cell transplantation as an initiator of endogenous stem cell-based tissue repair. *Curr Opin Organ Transplant* 17: 670-4, 2012.
24. Down JD, Yanch JC. Identifying the high radiosensitivity of the lungs of C57L mice in a model of total-body irradiation and bone marrow transplantation. *Radiat Res* 174: 258-63, 2010.
25. Eldh T, Heinzelmann F, Velalakan A, Budach W, Belka C, Jendrossek V. Radiation-induced changes in breathing frequency and lung histology of C57BL/6J mice are time- and dose-dependent. *Strahlenther Onkol* 188: 274-81, 2012.
26. Ergun S, Tilki D, Klein D. Vascular wall as a reservoir for different types of stem and progenitor cells. *Antioxid Redox Signal* 15: 981-95, 2011.
27. Fajardo LF. The pathology of ionizing radiation as defined by morphologic patterns. *Acta Oncol* 44: 13-22, 2005.
28. Fukai T, Ushio-Fukai M. Superoxide dismutases: role in redox signaling, vascular function, and diseases. *Antioxid Redox Signal* 15: 1583-606, 2011.
29. Gao F, Fish BL, Szabo A, Doctrow SR, Kma L, Molthen RC, Moulder JE, Jacobs ER, Medhora M. Short-term treatment with a SOD/catalase mimetic, EUK-207, mitigates pneumonitis and fibrosis after single-dose total-body or whole-thoracic irradiation. *Radiat Res* 178: 468-80, 2012.
30. Gao F, Kinnula VL, Myllarniemi M, Oury TD. Extracellular superoxide dismutase in pulmonary fibrosis. *Antioxid Redox Signal* 10: 343-54, 2008.
31. Garcia-Barros M, Paris F, Cordon-Cardo C, Lyden D, Rafii S, Haimovitz-Friedman A, Fuks Z, Kolesnick R. Tumor response to radiotherapy regulated by endothelial cell apoptosis. *Science* 300: 1155-9, 2003.
32. Ghafoori P, Marks LB, Vujaskovic Z, Kelsey CR. Radiation-induced lung injury. Assessment, management, and prevention. *Oncology (Williston Park)* 22: 37-47; discussion 52-3, 2008.
33. Ghobadi G, van der Veen S, Bartelds B, de Boer RA, Dickinson MG, de Jong JR, Faber H, Niemantsverdriet M, Brandenburg S, Berger RM, Langendijk JA, Coppes RP, van Luijk P. Physiological interaction of heart and lung in thoracic irradiation. *Int J Radiat Oncol Biol Phys* 84: e639-46, 2012.
34. Ghosh SN, Wu Q, Mader M, Fish BL, Moulder JE, Jacobs ER, Medhora M, Molthen RC. Vascular injury after whole thoracic x-ray irradiation in the rat. *Int J Radiat Oncol Biol Phys* 74: 192-9, 2009.
35. Gibbons MA, MacKinnon AC, Ramachandran P, Dhaliwal K, Duffin R, Phythian-Adams AT, van Rooijen N, Haslett C, Howie SE, Simpson AJ, Hirani N, Gauldie J, Iredale JP, Sethi T, Forbes SJ. Ly6Chi monocytes direct alternatively activated profibrotic macrophage regulation of lung fibrosis. *Am J Respir Crit Care Med* 184: 569-81, 2011.
36. Gnecchi M, Zhang Z, Ni A, Dzau VJ. Paracrine mechanisms in adult stem cell signaling and therapy. *Circ Res* 103: 1204-19, 2008.

37. Graves PR, Siddiqui F, Anscher MS, Movsas B. Radiation pulmonary toxicity: from mechanisms to management. *Semin Radiat Oncol* 20: 201-7, 2010.
38. Guckenberger M, Baier K, Polat B, Richter A, Krieger T, Wilbert J, Mueller G, Flentje M. Dose-response relationship for radiation-induced pneumonitis after pulmonary stereotactic body radiotherapy. *Radiother Oncol* 97: 65-70, 2010.
39. Jun D, Garat C, West J, Thorn N, Chow K, Cleaver T, Sullivan T, Torchia EC, Childs C, Shade T, Tadjali M, Lara A, Nozik-Grayck E, Malkoski S, Sorrentino B, Meyrick B, Klemm D, Rojas M, Wagner DH, Jr., Majka SM. The pathology of bleomycin-induced fibrosis is associated with loss of resident lung mesenchymal stem cells that regulate effector T-cell proliferation. *Stem Cells* 29: 725-35, 2011.
40. Kelsey CR, Horwitz ME, Chino JP, Craciunescu O, Steffey B, Folz RJ, Chao NJ, Rizzieri DA, Marks LB. Severe pulmonary toxicity after myeloablative conditioning using total body irradiation: an assessment of risk factors. *Int J Radiat Oncol Biol Phys* 81: 812-8, 2011.
41. Kishaba Y, Matsubara D, Niki T. Heterogeneous expression of nestin in myofibroblasts of various human tissues. *Pathol Int* 60: 378-85, 2010.
42. Klein D. Vascular Wall-Resident Multipotent Stem Cells of Mesenchymal Nature within the Process of Vascular Remodeling: Cellular Basis, Clinical Relevance, and Implications for Stem Cell Therapy. *Stem Cells Int* 2016: 1905846, 2016.
43. Klein D, Meissner N, Kleff V, Jastrow H, Yamaguchi M, Ergun S, Jendrossek V. Nestin(+) tissue-resident multipotent stem cells contribute to tumor progression by differentiating into pericytes and smooth muscle cells resulting in blood vessel remodeling. *Front Oncol* 4: 169, 2014.
44. Klein D, Schmetter A, Imsak R, Wirsdorfer F, Unger K, Jastrow H, Stuschke M, Jendrossek V. Therapy with Multipotent Mesenchymal Stromal Cells Protects Lungs from Radiation-Induced Injury and Reduces the Risk of Lung Metastasis. *Antioxid Redox Signal* 24: 53-69, 2016.
45. Klein D, Schmitz T, Verhelst V, Panic A, Schenck M, Reis H, Drab M, Sak A, Herskind C, Maier P, Jendrossek V. Endothelial Caveolin-1 regulates the radiation response of epithelial prostate tumors. *Oncogenesis* 4: e148, 2015.
46. Koukourakis MI. Radiation damage and radioprotectants: new concepts in the era of molecular medicine. *Br J Radiol* 85: 313-30, 2012.
47. Lakhdar R, Denden S, Kassab A, Leban N, Knani J, Lefranc G, Miled A, Chibani JB, Khelil AH. Update in chronic obstructive pulmonary disease: role of antioxidant and metabolizing gene polymorphisms. *Exp Lung Res* 37: 364-75, 2011.
48. Langan AR, Khan MA, Yeung IW, Van Dyk J, Hill RP. Partial volume rat lung irradiation: the protective/mitigating effects of Eukarion-189, a superoxide dismutase-catalase mimetic. *Radiother Oncol* 79: 231-8, 2006.
49. Mahmood J, Jelveh S, Calveley V, Zaidi A, Doctrow SR, Hill RP. Mitigation of radiation-induced lung injury by genistein and EUK-207. *Int J Radiat Biol* 87: 889-901, 2011.
50. Maiolica A, Borsotti D, Rappsilber J. Self-made frits for nanoscale columns in proteomics. *Proteomics* 5: 3847-50, 2005.
51. Makinde AY, John-Aryankalayil M, Palayoor ST, Cerna D, Coleman CN. Radiation survivors: understanding and exploiting the phenotype following fractionated radiation therapy. *Mol Cancer Res* 11: 5-12, 2013.
52. Marriott S, Baskir RS, Gaskill C, Menon S, Carrier EJ, Williams J, Talati M, Helm K, Alford CE, Kropski JA, Loyd J, Wheeler L, Johnson J, Austin E, Nozik-Grayck E, Meyrick B, West JD, Klemm DJ, Majka SM. ABCG2pos lung mesenchymal stem cells are a novel pericyte subpopulation that contributes to fibrotic remodeling. *Am J Physiol Cell Physiol* 307: C684-98, 2014.
53. Martin J, Helm K, Ruegg P, Varella-Garcia M, Burnham E, Majka S. Adult lung side population cells have mesenchymal stem cell potential. *Cytotherapy* 10: 140-51, 2008.
54. McNulty K, Janes SM. Stem cells and pulmonary fibrosis: cause or cure? *Proc Am Thorac Soc* 9: 164-71, 2012.
55. McQualter JL, Brouard N, Williams B, Baird BN, Sims-Lucas S, Yuen K, Nilsson SK, Simmons PJ, Bertoncello I. Endogenous fibroblastic progenitor cells in the adult mouse lung are highly enriched in the sca-1 positive cell fraction. *Stem Cells* 27: 623-33, 2009.
56. Michalski A, Damoc E, Lange O, Denisov E, Nolting D, Muller M, Viner R, Schwartz J, Remes P, Belford M, Dunyach JJ, Cox J, Horning S, Mann M, Makarov A. Ultra high resolution linear ion trap Orbitrap mass spectrometer (Orbitrap Elite) facilitates top down LC MS/MS and versatile peptide fragmentation modes. *Mol Cell Proteomics* 11: O111 013698, 2012.
57. Milliat F, Francois A, Tamarat R, Benderitter M. [Role of endothelium in radiation-induced normal tissue damages]. *Ann Cardiol Angeiol (Paris)* 57: 139-48, 2008.

Mesenchymal stem cell therapy protects lungs from radiation-induced endothelial cell loss by restoring superoxide dismutase 1 expression (doi: 10.1089/ars.2016.6748)
This paper has been peer-reviewed and accepted for publication, but has yet to undergo copyediting and proof correction. The final published version may differ from this proof.

58. Moulder JE, Cohen EP. Future strategies for mitigation and treatment of chronic radiation-induced normal tissue injury. *Semin Radiat Oncol* 17: 141-8, 2007.
59. Niki E. Antioxidants: basic principles, emerging concepts, and problems. *Biomed J* 37: 106-11, 2014.
60. Olsen JV, de Godoy LM, Li G, Macek B, Mortensen P, Pesch R, Makarov A, Lange O, Horning S, Mann M. Parts per million mass accuracy on an Orbitrap mass spectrometer via lock mass injection into a C-trap. *Mol Cell Proteomics* 4: 2010-21, 2005.
61. Paris F, Fuks Z, Kang A, Capodieci P, Juan G, Ehleiter D, Haimovitz-Friedman A, Cordon-Cardo C, Kolesnick R. Endothelial apoptosis as the primary lesion initiating intestinal radiation damage in mice. *Science* 293: 293-7, 2001.
62. Park MT, Oh ET, Song MJ, Lee H, Park HJ. Radio-sensitivities and angiogenic signaling pathways of irradiated normal endothelial cells derived from diverse human organs. *J Radiat Res* 53: 570-80, 2012.
63. Pilling D, Gomer RH. Persistent lung inflammation and fibrosis in serum amyloid P component (APCs-/-) knockout mice. *PLoS One* 9: e93730, 2014.
64. Prasanna SJ, Gopalakrishnan D, Shankar SR, Vasandan AB. Pro-inflammatory cytokines, IFNgamma and TNFalpha, influence immune properties of human bone marrow and Wharton jelly mesenchymal stem cells differentially. *PLoS One* 5: e9016, 2010.
65. Reddy SP. The antioxidant response element and oxidative stress modifiers in airway diseases. *Curr Mol Med* 8: 376-83, 2008.
66. Ribeiro A, Laranjeira P, Mendes S, Velada I, Leite C, Andrade P, Santos F, Henriques A, Graos M, Cardoso CM, Martinho A, Pais M, da Silva CL, Cabral J, Trindade H, Paiva A. Mesenchymal stem cells from umbilical cord matrix, adipose tissue and bone marrow exhibit different capability to suppress peripheral blood B, natural killer and T cells. *Stem Cell Res Ther* 4: 125, 2013.
67. Rolandsson S, Andersson Sjoland A, Brune JC, Li H, Kassem M, Mertens F, Westergren A, Eriksson L, Hansson L, Skog I, Bjermer L, Scheding S, Westergren-Thorsson G. Primary mesenchymal stem cells in human transplanted lungs are CD90/CD105 perivascularly located tissue-resident cells. *BMJ Open Respir Res* 1: e000027, 2014.
68. Rosenthal RA, Fish B, Hill RP, Huffman KD, Lazarova Z, Mahmood J, Medhora M, Molthen R, Moulder JE, Sonis ST, Tofilon PJ, Doctrow SR. Salen Mn complexes mitigate radiation injury in normal tissues. *Anticancer Agents Med Chem* 11: 359-72, 2011.
69. Rube CE, Uthe D, Wilfert F, Ludwig D, Yang K, Konig J, Palm J, Schuck A, Willich N, Remberger K, Rube C. The bronchiolar epithelium as a prominent source of pro-inflammatory cytokines after lung irradiation. *Int J Radiat Oncol Biol Phys* 61: 1482-92, 2005.
70. Scobioala S, Klocke R, Kuhlmann M, Tian W, Hasib L, Milting H, Koenig S, Stelljes M, El-Banayosy A, Tenderich G, Michel G, Breithardt G, Nikol S. Up-regulation of nestin in the infarcted myocardium potentially indicates differentiation of resident cardiac stem cells into various lineages including cardiomyocytes. *FASEB J* 22: 1021-31, 2008.
71. Shah MH, Liu GS, Thompson EW, Dusting GJ, Peshavariya HM. Differential effects of superoxide dismutase and superoxide dismutase/catalase mimetics on human breast cancer cells. *Breast Cancer Res Treat* 150: 523-34, 2015.
72. Siani A, Tirelli N. Myofibroblast differentiation: main features, biomedical relevance, and the role of reactive oxygen species. *Antioxid Redox Signal* 21: 768-85, 2014.
73. Sinclair KA, Yerkovich ST, Chen T, McQualter JL, Hopkins PM, Wells CA, Chambers DC. Mesenchymal Stromal Cells are Readily Recoverable from Lung Tissue, but Not the Alveolar Space, in Healthy Humans. *Stem Cells*, 2016.
74. Stenmark KR, Fagan KA, Frid MG. Hypoxia-induced pulmonary vascular remodeling: cellular and molecular mechanisms. *Circ Res* 99: 675-91, 2006.
75. Stewart DJ, Mei SH. Cell-based therapies for lung vascular diseases: lessons for the future. *Proc Am Thorac Soc* 8: 535-40, 2011.
76. Tsoutsou PG, Koukourakis MI. Radiation pneumonitis and fibrosis: mechanisms underlying its pathogenesis and implications for future research. *Int J Radiat Oncol Biol Phys* 66: 1281-93, 2006.
77. Tzouvelekis A, Koliakos G, Ntolios P, Baira I, Bouros E, Oikonomou A, Zissimopoulos A, Kolios G, Kakagia D, Paspaliaris V, Kotsianidis I, Froudarakis M, Bouros D. Stem cell therapy for idiopathic pulmonary fibrosis: a protocol proposal. *J Transl Med* 9: 182, 2011.
78. Tzouvelekis A, Ntolios P, Bouros D. Stem cell treatment for chronic lung diseases. *Respiration* 85: 179-92, 2013.
79. Vorotnikova E, Rosenthal RA, Tries M, Doctrow SR, Braunhut SJ. Novel synthetic SOD/catalase mimetics can mitigate capillary endothelial cell apoptosis caused by ionizing radiation. *Radiat Res* 173: 748-59, 2010.

Mesenchymal stem cell therapy protects lungs from radiation-induced endothelial cell loss by restoring superoxide dismutase 1 expression (doi: 10.1089/ars.2016.6748)
This paper has been peer-reviewed and accepted for publication, but has yet to undergo copyediting and proof correction. The final published version may differ from this proof.

80. Vujaskovic Z, Batinic-Haberle I, Rabbani ZN, Feng QF, Kang SK, Spasojevic I, Samulski TV, Fridovich I, Dewhirst MW, Anscher MS. A small molecular weight catalytic metalloporphyrin antioxidant with superoxide dismutase (SOD) mimetic properties protects lungs from radiation-induced injury. *Free Radic Biol Med* 33: 857-63, 2002.
81. Wirsdorfer F, Cappuccini F, Niazman M, de Leve S, Westendorf AM, Ludemann L, Stuschke M, Jendrossek V. Thorax irradiation triggers a local and systemic accumulation of immunosuppressive CD4+ FoxP3+ regulatory T cells. *Radiat Oncol* 9: 98, 2014.
82. Wirsdorfer F, de Leve S, Cappuccini F, Eldh T, Meyer AV, Gau E, Thompson LF, Chen NY, Karmouty-Quintana H, Fischer U, Kasper M, Klein D, Ritchey JW, Blackburn MR, Westendorf AM, Stuschke M, Jendrossek V. Extracellular adenosine production by ecto-5'-nucleotidase (CD73) enhances radiation-induced lung fibrosis. *Cancer Res*, 2016.
83. Yamaguchi M. Analysis of neurogenesis using transgenic mice expressing GFP with nestin gene regulatory regions. *Chem Senses* 30 Suppl 1: i117-8, 2005.
84. Zeng L, Ou G, Itasaka S, Harada H, Xie X, Shibuya K, Kizaka-Kondoh S, Morinibu A, Shinomiya K, Hiraoka M. TS-1 enhances the effect of radiotherapy by suppressing radiation-induced hypoxia-inducible factor-1 activation and inducing endothelial cell apoptosis. *Cancer Sci* 99: 2327-35, 2008.
85. Zhang L, Dong XW, Wang JN, Tang JM, Yang JY, Guo LY, Zheng F, Kong X, Huang YZ, Chen SY. PEP-1-CAT-transduced mesenchymal stem cells acquire an enhanced viability and promote ischemia-induced angiogenesis. *PLoS One* 7: e52537, 2012.
86. Zhang ZY, Teoh SH, Chong MS, Schantz JT, Fisk NM, Choolani MA, Chan J. Superior osteogenic capacity for bone tissue engineering of fetal compared with perinatal and adult mesenchymal stem cells. *Stem Cells* 27: 126-37, 2009.
87. Zhao W, Robbins ME. Inflammation and chronic oxidative stress in radiation-induced late normal tissue injury: therapeutic implications. *Curr Med Chem* 16: 130-43, 2009.

Figure legends

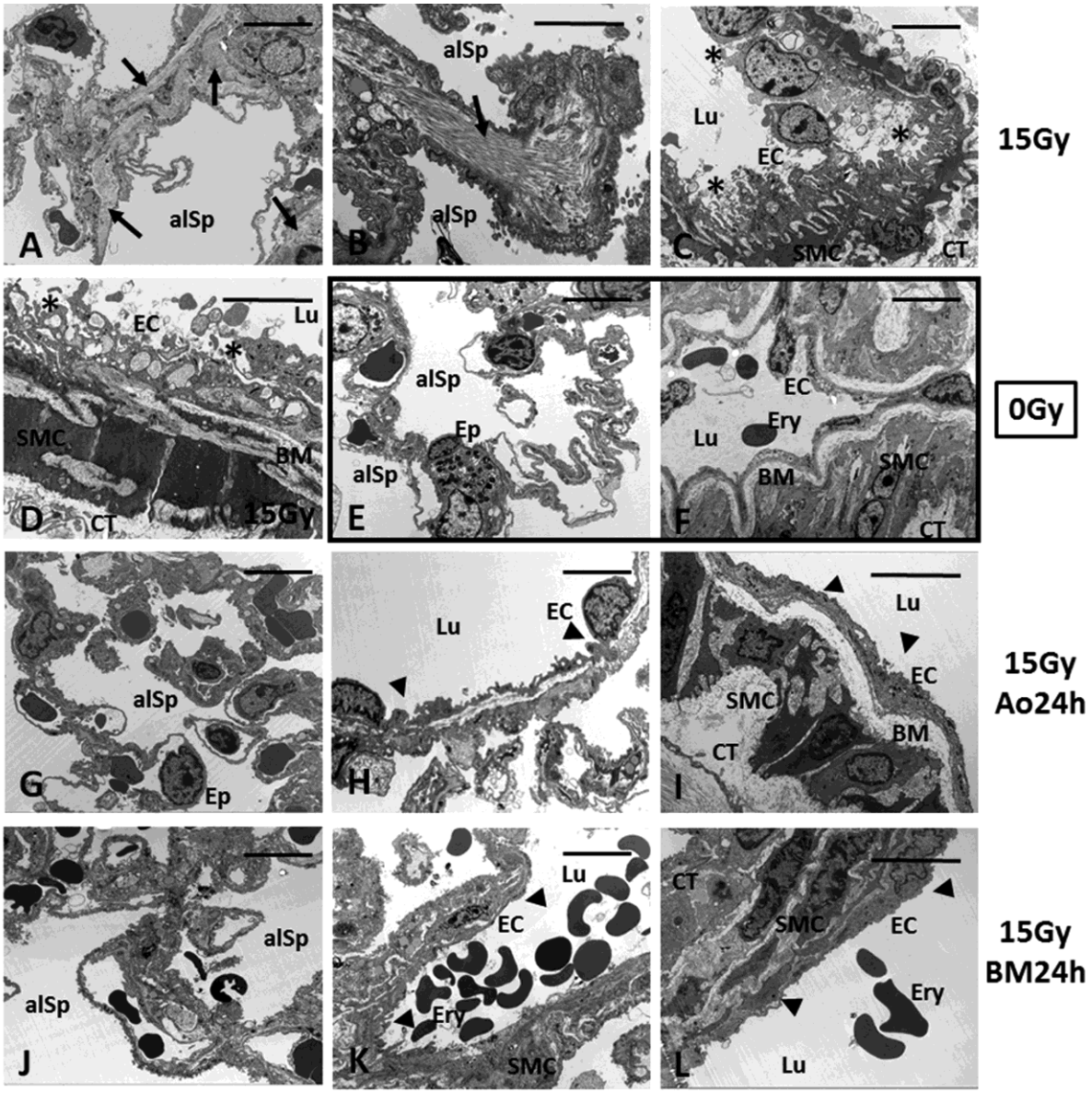

Figure 1

Thorax-irradiation induces late vascular EC damage whereas MSC-therapy normalizes EC morphology

C57BL/6 mice were left untreated or received a 15Gy WTI. Single cell suspensions of cultured MSCs ($0.5*10^6$ cells) derived from the aorta (Ao) or from the bone marrow (BM) were intravenously transplanted into the tail vein of control or WTI mice 24 hours after irradiation. Morphological analysis of lung blood vessels was done using electron microscopy 25 weeks post irradiation (n=3 per group). Massive collagen deposition in WTI lungs (15 Gy) are emphasized by arrows (A, B). Partially degraded mitochondria and numerous vacuoles present in endothelial cells (EC) are predominant in WTI lungs (C, D emphasized by

asterisks) as compared to sham controls (0Gy) (E, F marked by the black border). A regular vessel structure as well as EC morphology was present in the lungs of MSC-treated animals (emphasized by arrowheads) (G-L). alSp alveolar space, SMC smooth muscle cell, BM basement membrane, CT connective tissue, Lu lumen, Ery erythrocytes. Scale bar A-C, E, G, J = 20 µm, D, F, H, I, K, L = 10 µm.

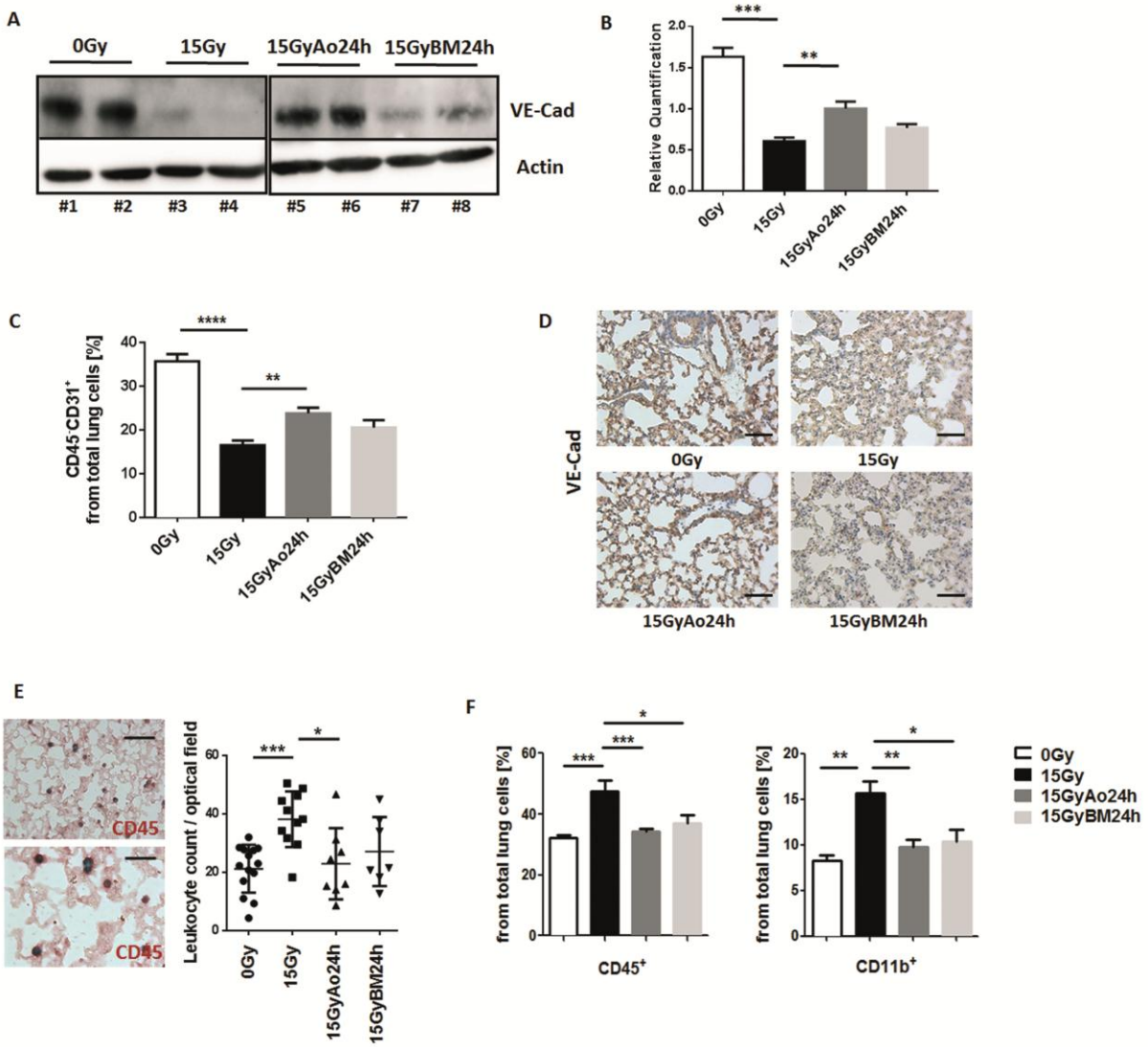

Figure 2

MSC-therapy limits radiation-induced EC loss as adverse late effect and associated immune cell infiltration

C57BL/6 mice were left untreated or received a 15Gy WTI and were subsequently transplanted with cultured Ao or BM MSCs ($0.5*10^6$ cells) 24 hours after irradiation as indicated. (A) Endothelial VE-Cadherin (VE-Cad) expression was analyzed in whole protein lysates using Western blot analysis at 25 weeks post irradiation. Representative blots from four different experiments are shown. (B) For quantification blots were analyzed by densitometry and the VE-Cad signal was related to beta-actin. P-values were indicated: $^{**}P \leq 0.01$; $^{***}P \leq 0.001$; by one-way ANOVA followed by post-hoc Tukey test (comparison to 15Gy). (C) EC were further quantified using FACS analysis and CD31 expression in the

Mesenchymal stem cell therapy protects lungs from radiation-induced endothelial cell loss by restoring superoxide dismutase 1 expression (doi: 10.1089/ars.2016.6748)
This paper has been peer-reviewed and accepted for publication, but has yet to undergo copyediting and proof correction. The final published version may differ from this proof.

absence of CD45 expression ($CD45^-CD31^+$ cells). Data are presented as mean ±SEM from two independent experiments (n = 6 mice per group). P-values were indicated: $^{**}P \leq 0.01$, $^{****}P \leq 0.0001$ as analyzed by one-way ANOVA followed by post-hoc Tukey's test. (D) Lungs were dissected 25 weeks after WTI and subjected to IHC analysis. Vessels were stained for VE-Cad using DAB staining (brown). Nuclei were counterstained with Hemalaun (blue). Representative lung photographs from five different mice are shown. Scale bar: 50µm. (E) Infiltrating $CD45^+$ leukocytes were quantified by counting numbers of specific CD45-positive immunoreactive structures (shown in red as visualized with alkaline phosphatase) in four randomly chosen optical fields. Representative staining from a WTI lung specimen was included as an example. Data are presented as mean ±SEM from four independent experiments. P-values were indicated: $^{*}P \leq 0.05$, $^{**}P < 0.01$ by one-way ANOVA followed by post-hoc Tukey's test (0Gy: n = 14; 15Gy: n = 11; 15GyAo24h: n = 8; 15GyBM24h: n = 7). Scale bar: 25µm (upper photo), 15µm (lower photo). (F) Infiltrating leukocytes/myeloid cells in crude cell extracts of freshly isolated lung tissue were further characterized using FACS analysis CD45 and CD11b antibodies. Data are presented as mean ± SEM (n = 4; 0Gy: n = 4; 15Gy: n = 6; 15GyAo24h: n = 7; 15GyBM24h: n = 4). P-values were indicated: $^{**}P \leq 0.01$, $^{***}P \leq 0.001$ as analyzed by one-way ANOVA followed by post-hoc Tukey's test.

"(To see this illustration in color the reader is referred to the web version of this article at www.liebertonline.com/ars)"

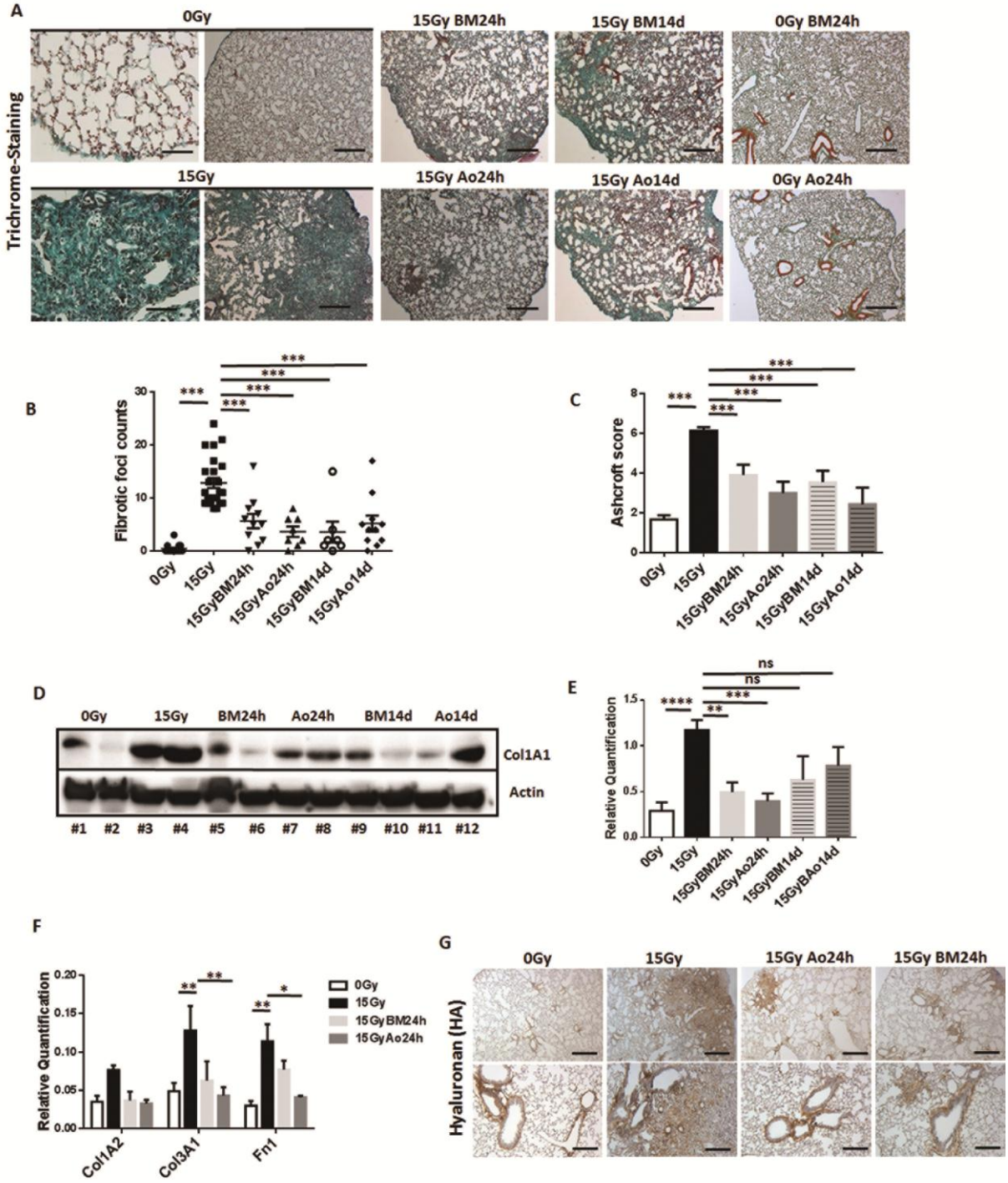

Figure 3

MSC-therapy limits radiation-induced lung fibrosis

C57BL/6 mice were left untreated or received a 15Gy WTI. Single cell suspensions of cultured MSCs ($0.5*10^6$ cells) derived from the aorta (Ao) or from the bone marrow (BM) were intravenously transplanted into the tail vein of control or WTI mice 24 hours or 14 days after irradiation as indicated. (A) Histological staining with Masson´s Goldner Trichrome on

Mesenchymal stem cell therapy protects lungs from radiation-induced endothelial cell loss by restoring superoxide dismutase 1 expression (doi: 10.1089/ars.2016.6748)
This paper has been peer-reviewed and accepted for publication, but has yet to undergo copyediting and proof correction. The final published version may differ from this proof.

sections of paraffin-embedded lung tissue was performed at 25 weeks after WTI. Sham irradiated (0Gy) animals which received cultured aortic or BM-MSC were included as control. Shown are representative light microscopy images (scale bar = 100µm and 25µm of higher magnifications). Quantification of lung fibrosis was done by counting the number of fibrotic foci (B) and furthermore by determining the Ashcroft scores (C) blinded to the genotype and treatment conditions. Data are presented as means ± SEM. ***$P \leq 0.001$ by one-way ANOVA followed by post-hoc Bonferroni test (0Gy: n = 15; 15Gy: n = 24; 15GyBM24h: n = 8; 15GyAo24h: n = 11; 15GyBM14d: n = 11; 15GyAo14d: n = 7). (D) Western blot analysis for Collagen (Col1A1) protein levels was further performed with whole protein lysates at 25 weeks post irradiation to confirm WTI-induced fibrosis development. (E) For quantification blots were analyzed by densitometry and the Collagen signal was related to beta-actin (0Gy: n = 8; 15Gy: n = 8; 15GyBM24h: n = 6; 15GyAo24h: n = 8; 15GyBM14d: n = 4; 15GyAo14d: n = 4). P-values were indicated: *$P \leq 0.05$, ***$P \leq 0.001$ ****$P \leq 0.0001$ by one-way ANOVA followed by post-hoc Tukey's test (comparison to 15Gy). (F) qRT-PCR quantifications of the extracellular matrix components Col1A2, Col3A1 and fibronectin 1 (Fn1) were performed and shown as relative expression to actin (0Gy: n = 5; 15Gy: n = 6; 15GyBM24h: n = 5; 15GyAo24h: n = 5) at ≥ 25 weeks post irradiation. Shown are mean values ± SEM from 5 independent samples per group measured in duplicates each. *$P \leq 0.05$, **$P \leq 0.01$, by one-way ANOVA followed by post-hoc Tukey's test. (G) The major extra cellular matrix glycosaminoglycan hyaluronan (HA) was further analyzed in lung section using DAB staining (brown). Nuclei were counterstained with Hemalaun (blue). Representative lung photographs from five different mice are shown. Scale bar = 100 µm.

"(To see this illustration in color the reader is referred to the web version of this article at www.liebertonline.com/ars)"

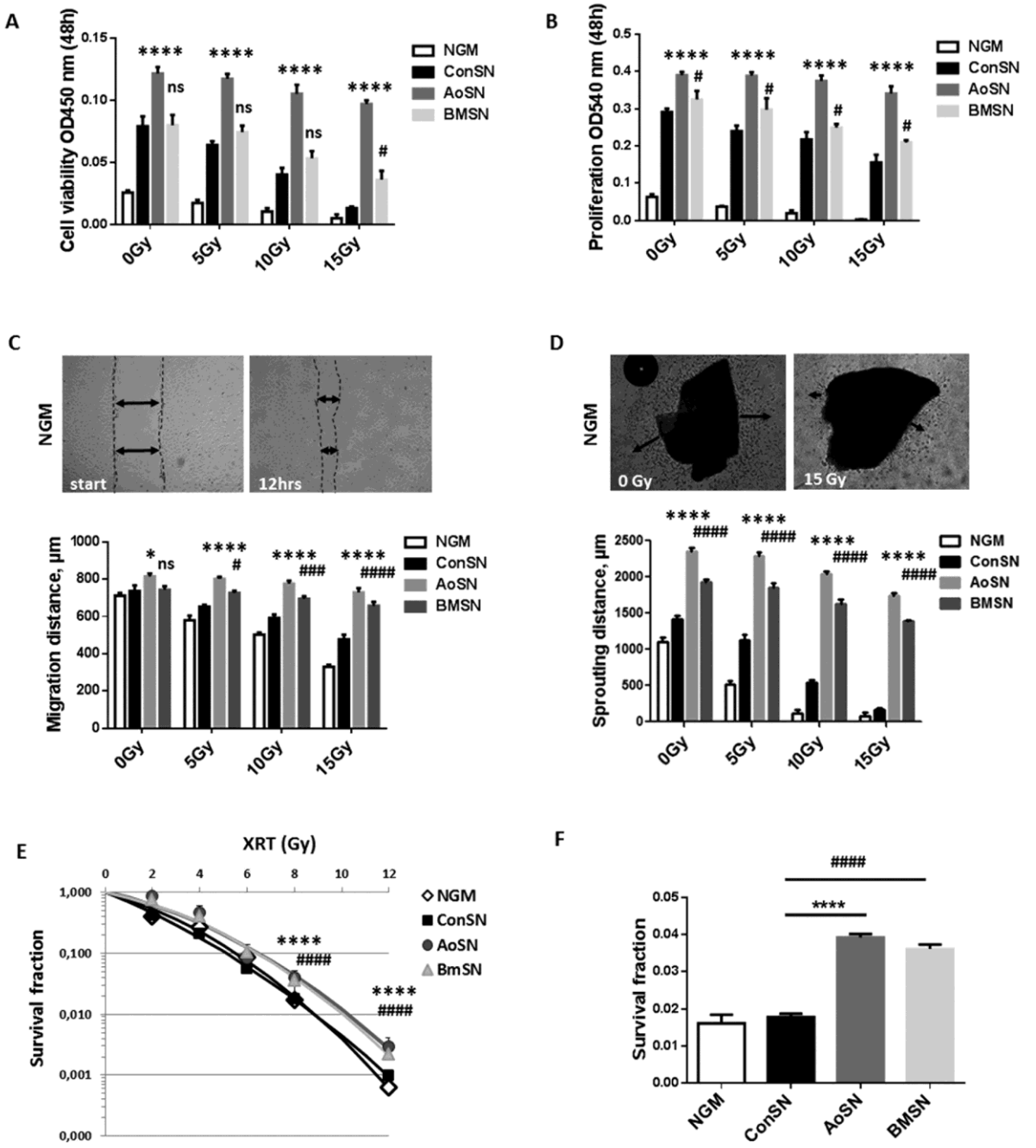

Figure 4

Treatment of cultured lung microvascular EC (LMEC) with MSCs-derived supernatants rescues radiation-induced alterations of EC behavior

(A) Cell viability of cultured LMECs was assessed after radiation with the indicated radiation doses and subsequent treatment of cells in normal growth medium (NGM), control supernatant (ConSN) or supernatants derived from cultured aortic MSCs (AoSN) and bone marrow MSCs (BMSN) using the WST-1 reagent. (B) Proliferation was further analyzed with

Mesenchymal stem cell therapy protects lungs from radiation-induced endothelial cell loss by restoring superoxide dismutase 1 expression (doi: 10.1089/ars.2016.6748)
This paper has been peer-reviewed and accepted for publication, but has yet to undergo copyediting and proof correction. The final published version may differ from this proof.

the crystal violet assay. Data are shown as means ± SEM of three independent experiments measured in quadruplets each. ****$P \leq 0.0001$, $^{\#}P \leq 0.05$ by one-way ANOVA followed by post-hoc Tukey's test (comparison to 15Gy; * AoSN, # BMSN). (C) LMEC migration was investigated after irradiation and subsequent introduction of a thin wound in confluent monolayers by scratching with a pipette tip. Wound closure was determined for the different treatments by measuring the migration distance after 8 hours. Data are shown as means ±SEM of three independent experiments measured in duplicates each. ****,$^{\#\#\#\#}P \leq 0.0001$, ***,$^{\#\#\#}P \leq 0.001$, **,$^{\#\#}P \leq 0.01$ *,$^{\#}P \leq 0.05$, (ns not significant) by one-way ANOVA followed by post-hoc Tukey's test (comparison to 15Gy; * AoSN, # BMSN). (D) EC sprouting was further determined using ex vivo isolated lung explants embedded in growth factor-reduced Matrigel in NGM supplemented with or without MSCs conditioned medium. Capillary-like outgrowth was quantified by measuring the sprouting distance 4 days post irradiation. Data are shown as means ±SEM of three independent experiments measured in duplicates each. ****, $^{\#\#\#\#}P \leq$ 0.0001 by one-way ANOVA followed by post-hoc Tukey's test (comparison to 15Gy; * AoSN, # BMSN). (E) LMECs were plated for colony formation assay, irradiated with indicated doses and subsequently further incubated with the indicated treatments for additional 10 days. (F) The survival fractions for the irradiations with 8Gy are further shown as bar blot. Data show the surviving fractions from three independent experiments measured in triplicates each (means ± SD). ****$P \leq 0.0001$ by one-way ANOVA followed by post-hoc Tukey's test (comparison to 15Gy; * AoSN, # BMSN).

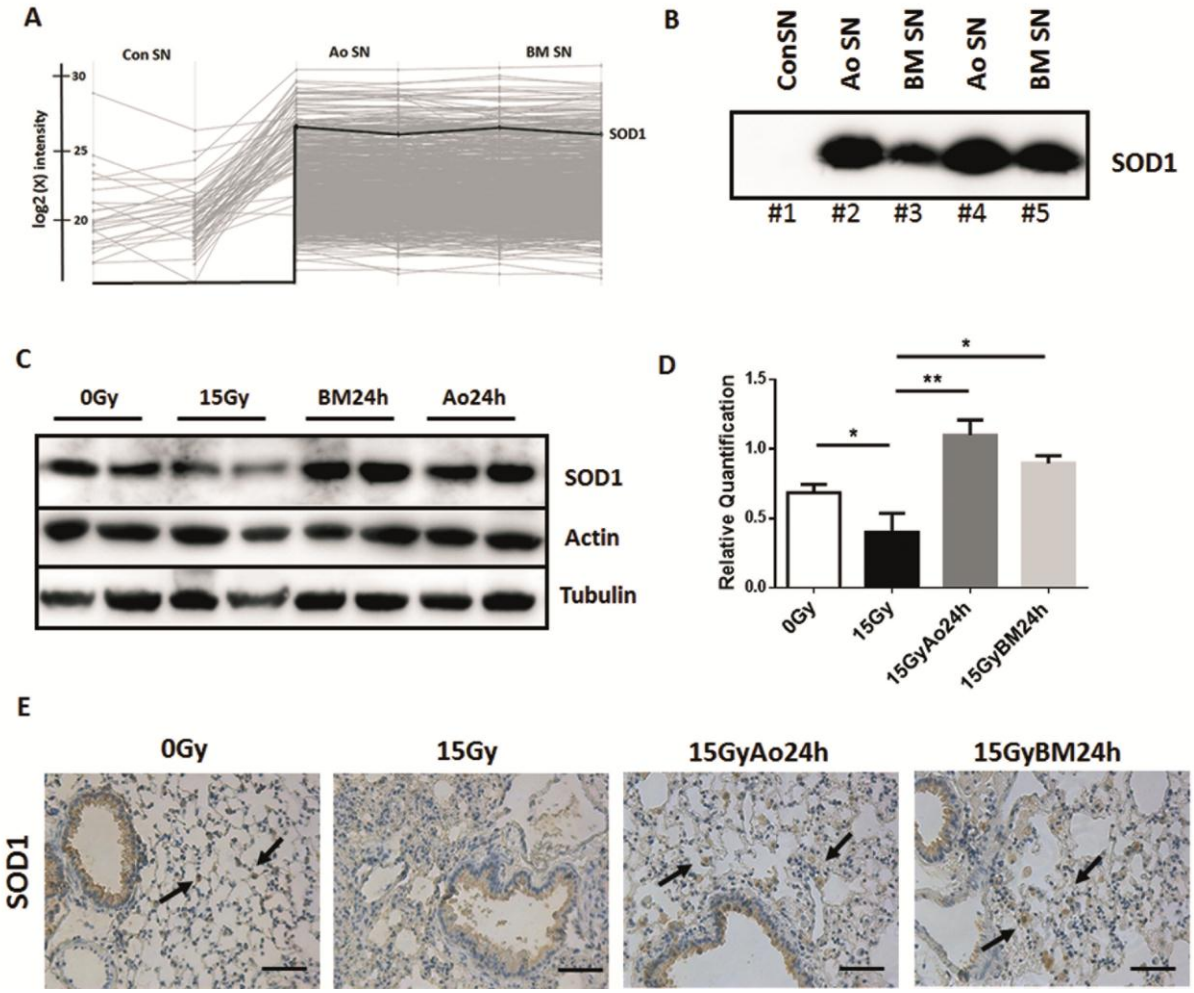

Figure 5

Therapeutically applied stem cells secrete SOD1 and restore SOD1 expression in WTI treated lungs

(A) Control supernatants (ConSN) and supernatants derived from cultured aortic MSCs (AoSN) and bone marrow MSCs (BMSN) were analyzed by label free quantitative mass spectrometry. Identified SOD1 protein in MSC supernatants is emphasized by a bold line. (B) SOD1 secretion of cultured MSCs was confirmed in cell culture derived supernatants using Western blot analysis. Equal protein amounts (50µg) were loaded. (C) SOD1 protein expression levels were further analyzed in whole protein lysates of control and WTI lungs with and without MSC treatment using Western blot analysis at 25 weeks post irradiation. Representative blots are shown. (B) For quantification blots were analyzed by densitometry and the SOD1 signal was related to beta-actin (n=4 for each group). P-values were indicated: $*P \leq 0.05$, $**P \leq 0.01$ by one-way ANOVA followed by post-hoc Tukey test (comparison to

15Gy). (E) Lung sections were further stained for SOD1 using DAB staining (brown). Nuclei were counterstained with Hemalaun (blue). Arrows point to single SOD1-immunoreactive cells. Representative lung photographs from five different mice are shown. Scale bar = 100 µm.

"(To see this illustration in color the reader is referred to the web version of this article at www.liebertonline.com/ars)"

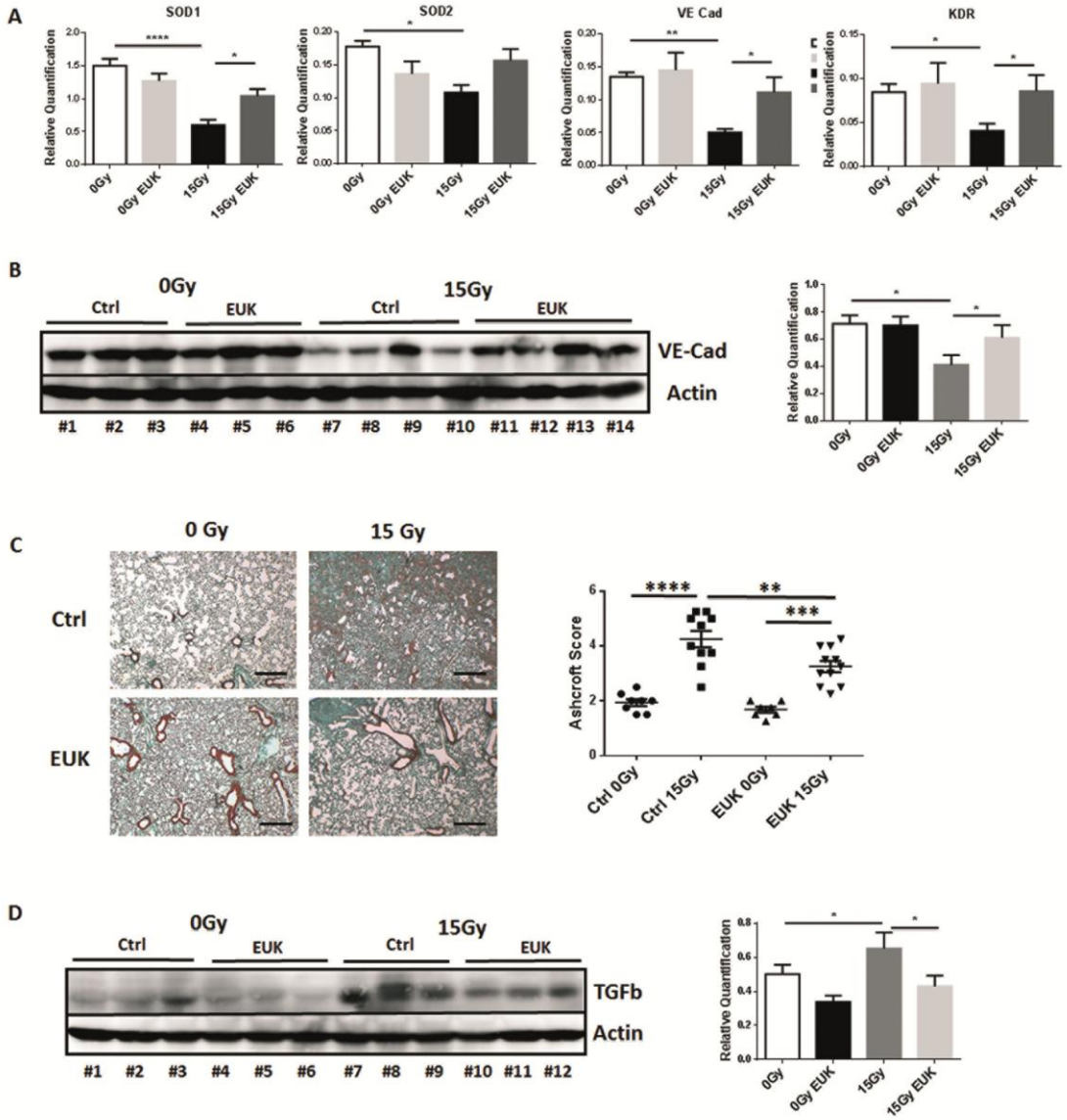

Figure 6

Treatment with superoxide dismutase mimetic counteracts radiation-induced EC loss and reduces lung fibrosis.

C57BL/6 mice irradiated with 0Gy or 15Gy WTI were subsequently treated three times a week (starting within 24 hours after WTI) within the first three weeks post-irradiation by intraperitoneal injection with 100 µl solvent (PBS) or 10 µg/g bodyweight of the superoxide dismutase mimetic EUK134 (diluted in 100µl PBS). Mice were sacrificed at 25-30 weeks post-irradiation and lung tissues were collected for further analysis. (A) qRT-PCR quantifications of SOD1 and SOD2 as well as for the EC marker VE-Cad and VEGFR2/KDR were performed and shown as relative expression to actin at ≥ 25 weeks post irradiation.

Mesenchymal stem cell therapy protects lungs from radiation-induced endothelial cell loss by restoring superoxide dismutase 1 expression (doi: 10.1089/ars.2016.6748)
This paper has been peer-reviewed and accepted for publication, but has yet to undergo copyediting and proof correction. The final published version may differ from this proof.

Shown are mean values ± SEM from 6 independent samples per group measured in duplicates each. **P* ≤ 0.05, ***P* ≤ 0.01, by one-way ANOVA followed by post-hoc Tukey's test. (B) Endothelial VE-Cadherin (VE-Cad) expression was analyzed in whole protein lysates using Western blot analysis at 25 weeks post irradiation. Representative blots from three different experiments are shown (0Gy: n=6, 0Gy EUK: n=6, 15Gy: n=8, 15Gy EUK: n=8). (B) For quantification blots were analyzed by densitometry and the VE-Cad signal was related to beta-actin. P-values were indicated: **P* ≤ 0.05, by one-way ANOVA followed by post-hoc Tukey test (comparison to 15Gy). (C) Histological staining with Masson´s Goldner Trichrome on sections of paraffin-embedded lung tissue was performed at 25 weeks after WTI. Shown are representative light microscopy images (scale bar = 100 µm and 25µm of higher magnifications). Quantification of lung fibrosis was done by determining the Ashcroft scores blinded to the genotype and treatment conditions. Data are presented as means ±SEM. ***P* ≤ 0.01 ****P* ≤ 0.001 *****P* ≤ 0.0001 by one-way ANOVA followed by post-hoc Bonferroni test (0Gy Ctrl: n=8, 0Gy EUK: n=7, 15Gy Ctrl: n=10, 15Gy EUK: n=11). (D) The pro-fibrotic cytokine transforming growth factor beta (TGFb) known to be associated with fibrosis development was further analyzed in whole protein lysates using Western blot analysis at 25 weeks post irradiation. Representative blots from three different experiments are shown (0Gy: n=6, 0Gy EUK: n=6, 15Gy: n=8, 15Gy EUK: n=8).

"(To see this illustration in color the reader is referred to the web version of this article at www.liebertonline.com/ars)"

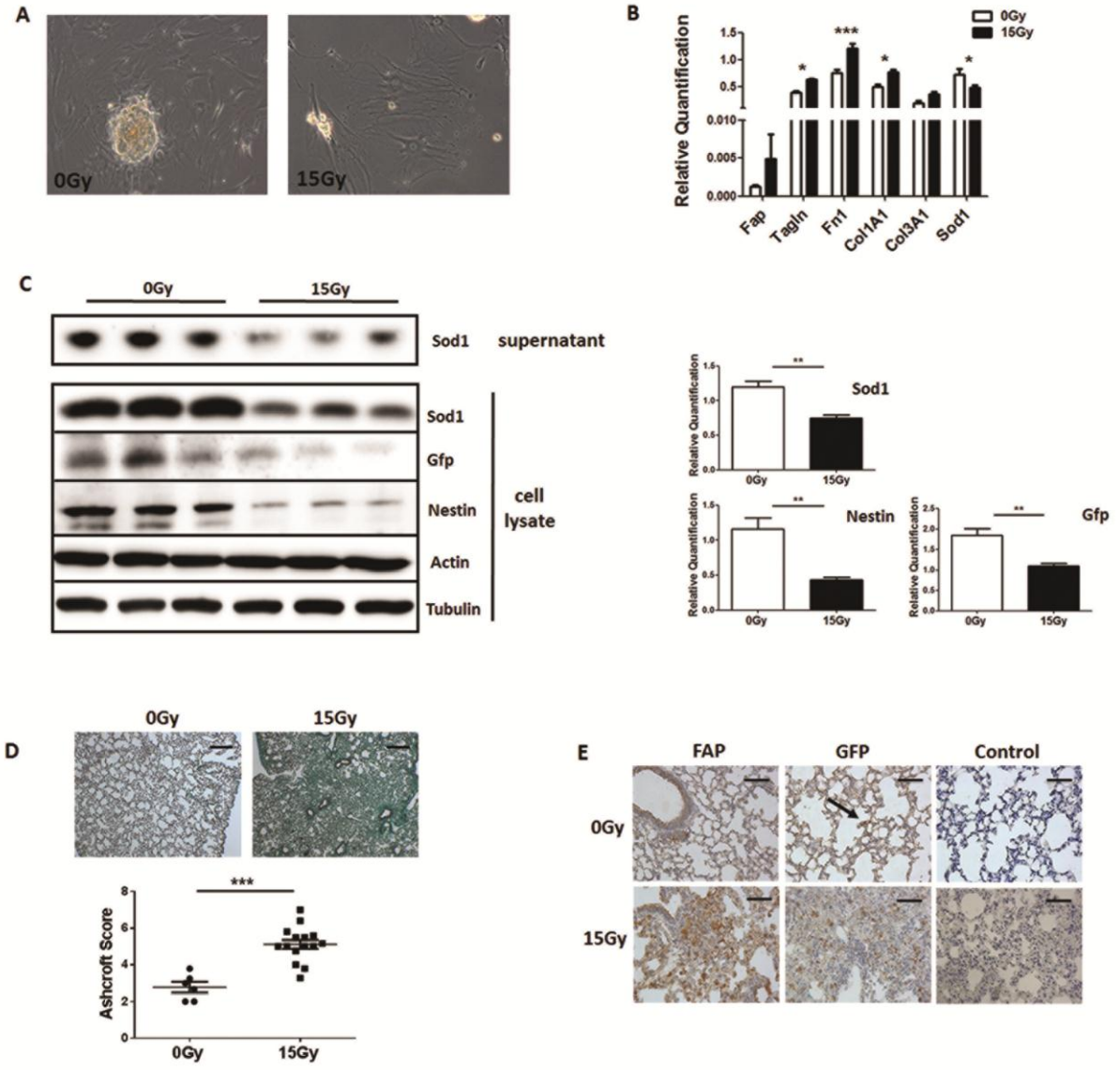

Figure 7

Radiation of cultured AoMSCs results in decreased expression levels of SOD1 and induces a fibroblast-like phenotype

(A) Phase contrast microscopy was performed in order to investigate the change of morphology in irradiated AoMSCs 96 hours after irradiation with 15Gy. Magnification: 40x. (B) qRT-PCR analysis was performed for the indicated fibroblast marker genes in cultured AoMSCs 96 hours after irradiation. Shown are mean values ±SEM from 4 independent samples per group measured in duplicates each. *$P \leq 0.05$, **$P \leq 0.01$, by one-way ANOVA followed by post-hoc Tukey's test. (C) Cultured AoMSCs derived from NestGFP transgenic mice were irradiated and after 96 hours total cell lysates as well as cell supernatants were

Mesenchymal stem cell therapy protects lungs from radiation-induced endothelial cell loss by restoring superoxide dismutase 1 expression (doi: 10.1089/ars.2016.6748)
This paper has been peer-reviewed and accepted for publication, but has yet to undergo copyediting and proof correction. The final published version may differ from this proof.

analyzed by Western blot for SOD1, GFP and Nestin expression. Representative blots from three different experiments are shown (n=3). For quantification blots were analyzed by densitometry and respective signals were related to beta-actin. P-values were indicated: ***P* ≤ 0.01, by two-tailed t-test. (D) NestGFP mice were left untreated or received a 15Gy WTI. Histological staining with Masson´s Goldner Trichrome on sections of paraffin-embedded lung tissue was performed at 25 weeks after WTI. Shown are representative light microscopy images (scale bar = 100µm). Quantification of lung fibrosis was done by determining the Ashcroft scores. Data are presented as means ±SEM. ****P* ≤ 0.001 by one-way ANOVA followed by post-hoc Bonferroni test (0Gy: n=6; 15Gy: n=15). (E) Lung sections were further stained for FAP and GFP using DAB staining (brown). Nuclei were counterstained with Hemalaun (blue). Representative lung photographs from five different mice are shown. Scale bar 50µm.

"(To see this illustration in color the reader is referred to the web version of this article at www.liebertonline.com/ars)"

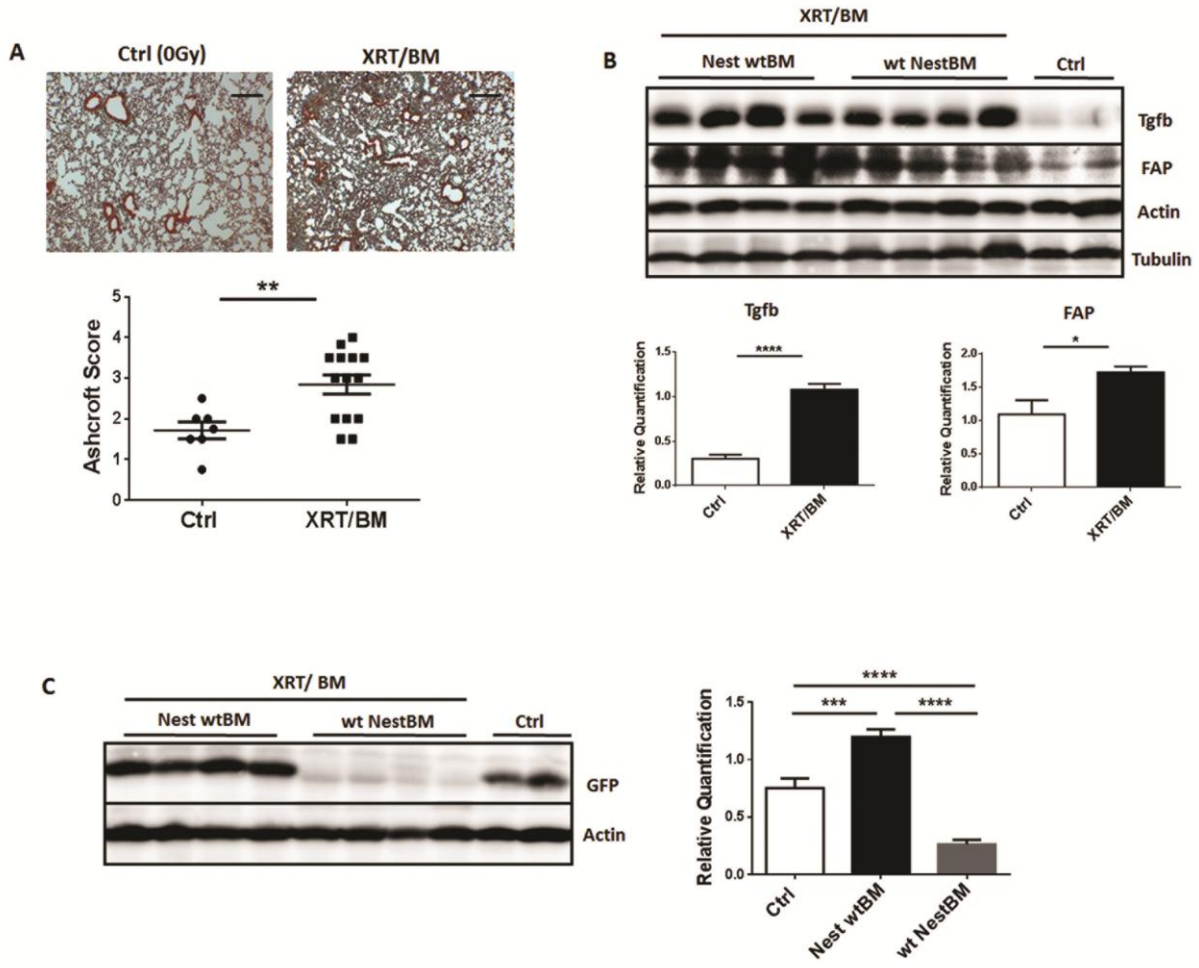

Figure 8

Tissue-resident NestGFP(+) cells and not BM-derived MSCs contribute to fibrosis development

NestGFP transgenic mice were lethally irradiated with a split dose of 7+3 Gy TBI and subsequently adoptively transferred with $2x10^6$ murine wt BM (XRT/BM) cells from C57BL/6 donor mice into the tail vain (Nest wtBM) and vice-versa (wt NestBM). Unirradiated NestGPF mice were used as Control [Ctrl (0Gy)]. (A) Histological staining with Masson´s Goldner Trichrome on sections of paraffin-embedded lung tissue was performed at 25 weeks after WTI. Shown are representative light microscopy images (scale bar = 100µm). Quantification of lung fibrosis was done by determining the Ashcroft scores. Data are presented as means ±SEM. $^{**}P \leq 0.01$ by one-way ANOVA followed by post-hoc Bonferroni test (Ctrl: n=7; XRT/BM: n=14). Tgfb1, FAP (B) and GFP (C) expressions were analyzed in whole protein lysates using Western blot analysis. Representative blots are shown. For quantification blots

were analyzed by densitometry and respective signals were related to beta-actin (n=7 for each group). **$P \leq 0.01$, ***$P \leq 0.001$, ****$P \leq 0.0001$ by one-way ANOVA followed by post-hoc Tukey test.

"(To see this illustration in color the reader is referred to the web version of this article at www.liebertonline.com/ars)"

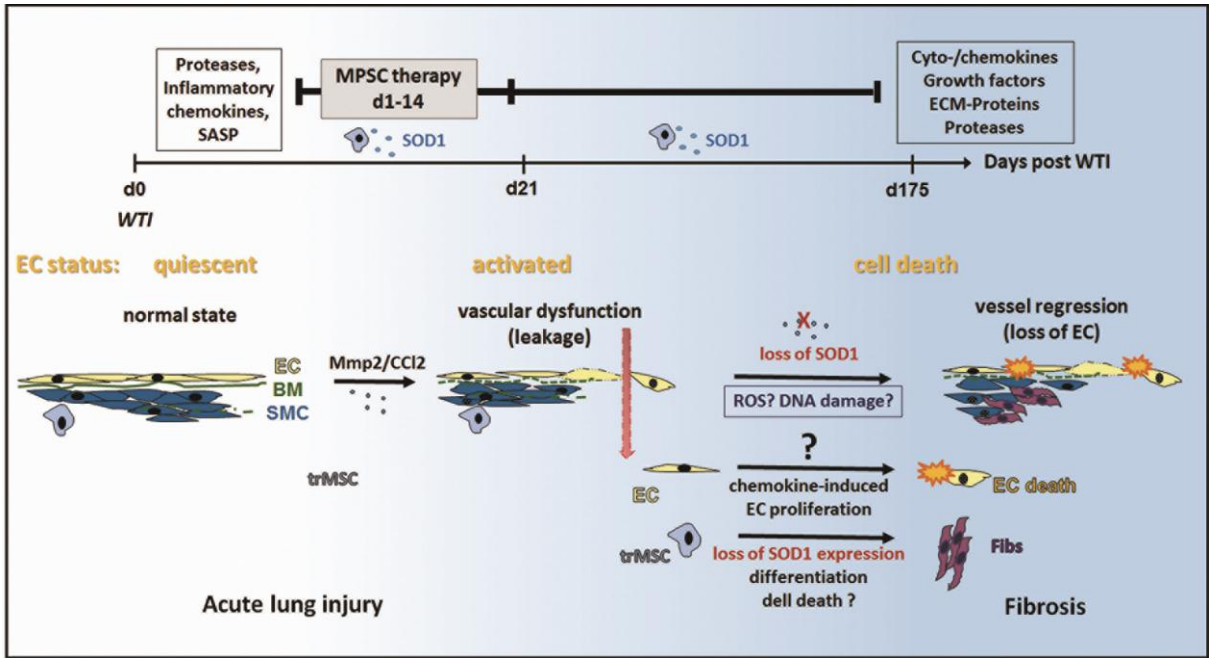

Figure 9

MSC therapy counteracts radiation-induced EC damage and EC loss

Usually in the healthy state EC are thought to be quiescent and thus normal lung capillaries providing an efficient barrier to liquids or cell extravasation. WTI considerably enhanced vascular leakage and this pro-invasive cellular activity was accompanied by radiation-induced EC damage and up-regulation of the endothelial matrix metalloproteinase Mmp2 as well as increased senescence-associated secretory phenotype (SASP) factor production Ccl2 by senescent bronchial-alveolar epithelial cells (44). As a long-term effect EC death occurs and this was accompanied by a reduced expression of the anti-oxidant protein superoxide dismutase 1 (SOD1). The radiation effects on EC were blocked by treating mice with cultured multipotent mesenchymal stromal cells (MPSCs) derived either from bone marrow (BM) or from aorta (Ao) within the first weeks after irradiation (pneumonitic phase) which have the potential to restore SOD1 expression levels in WTI lung tissue by a paracrine way of action. Putatively endogenous lung MSCs were protected hereby and thus do not contribute to fibrosis progression by differentiating into fibroblast-like cells. This study provides novel insight into the mechanisms of radiation-induced EC loss and potential protective strategies.

"(To see this illustration in color the reader is referred to the web version of this article at www.liebertonline.com/ars)"

Mesenchymal stem cell therapy protects lungs from radiation-induced endothelial cell loss by restoring superoxide dismutase 1 expression (doi: 10.1089/ars.2016.6748)
This paper has been peer-reviewed and accepted for publication, but has yet to undergo copyediting and proof correction. The final published version may differ from this proof.

Supplemental Material

Supplemental Figures

Figure S1

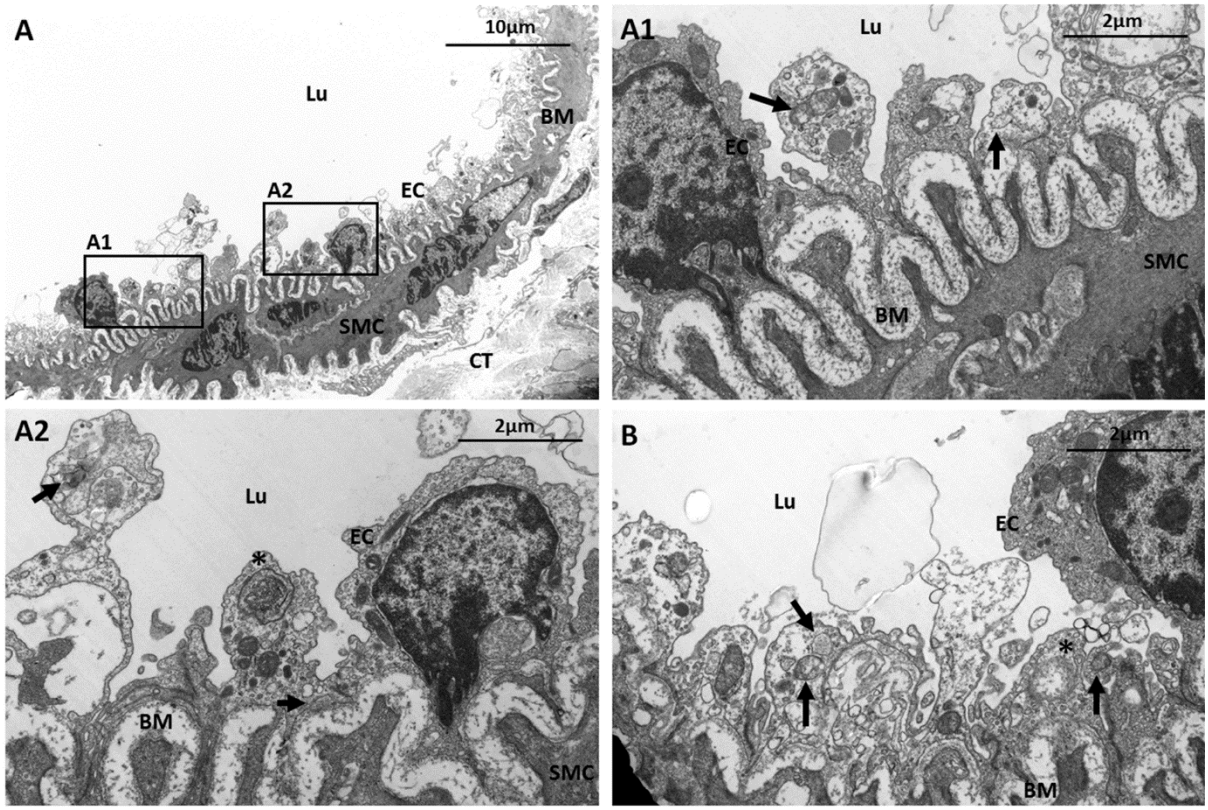

Thorax-irradiation induces late vascular EC damage

C57BL/6 mice received a 15Gy WTI. Morphological analysis of lung blood vessels was done using electron microscopy 25 weeks post irradiation (n=3 per group). (A, B). Partially degraded mitochondria (emphasized by arrows) and numerous vacuoles present in EC are predominant in WTI lungs. Presumably autophagosome/ autolysosome-like structures are emphasized by asterisks. alSp alveolar space, SMC smooth muscle cell, BM basement membrane, CT connective tissue, Lu lumen. Scale bars as indicated.

Figure S2

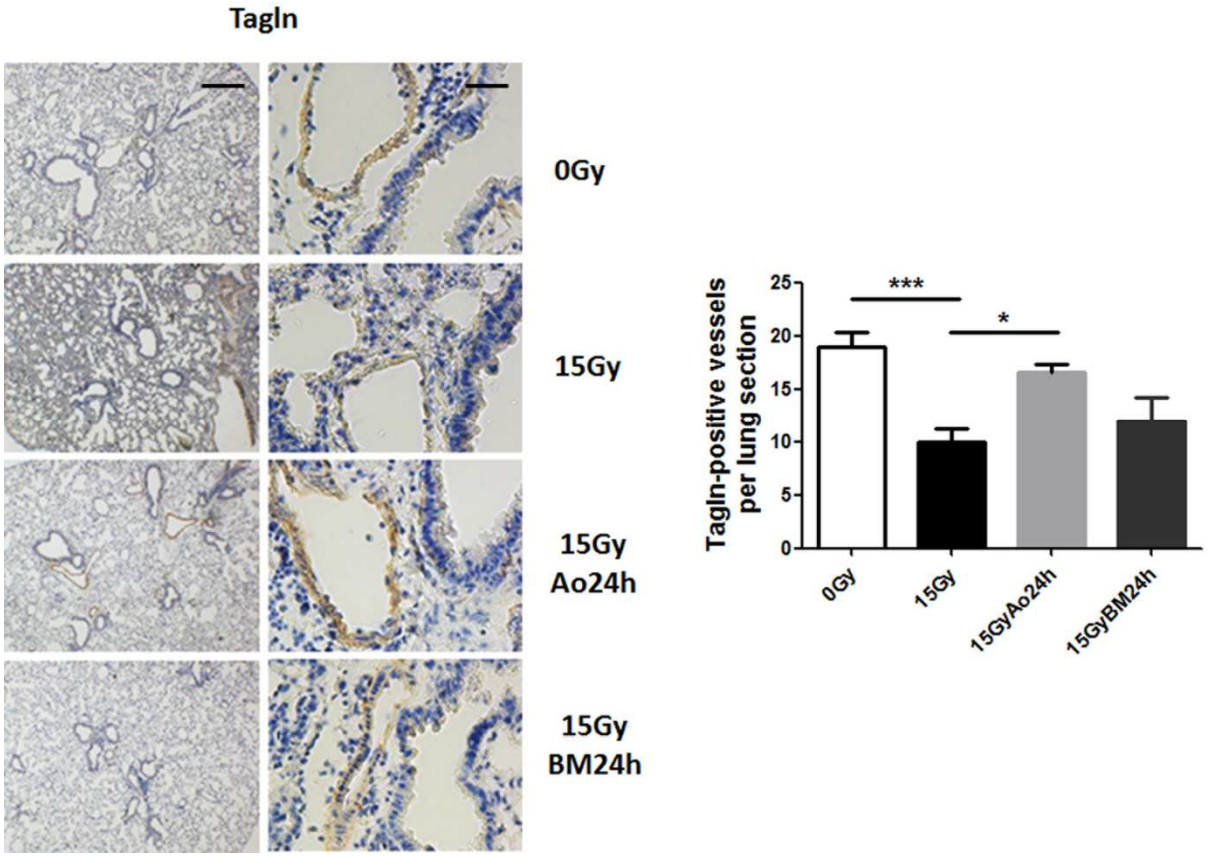

MSC-therapy limits radiation-induced EC loss as adverse late effect

C57BL/6 mice were left untreated or received a 15Gy WTI. Single cell suspensions of cultured AoMSCs or BM-MSCs ($0.5*10^6$ cells) were intravenously transplanted into the tail vein of control or WTI mice 24 hours after irradiation. (A) Lung sections were stained for tagln using DAB staining (brown) at 25 weeks after WTI. Shown are representative light microscopy images (scale bar = 100µm and 20µm of higher magnifications). Tagln-positive vessels were quantified by counting Tagln-immunoreactive vascular structures (SMC-stabilized vessels) in whole tissue sections. Therefore three to five 5 µm paraffin cross-sections were taken per mouse lung at the midpoint through the lung block depth and stained with Tagln antibody for histological evaluation. Samples were then analyzed microscopically with a 20× objective. Tagln-positive vessels were quantified by counting in at least 3 whole cross-sections per mice lung and averages for individual animals were calculated. Depicted data represent the mean values of all mice per group (mean of single average number for

each mice / mouse number) as indicated. *$P \leq 0.05$ ***$P \leq 0.001$ by one-way ANOVA followed by post-hoc Bonferroni test (0Gy: n=8; 15Gy: n=7; 15GyAo24h: n=5; 15GyBM24h: n=4).

Figure S3

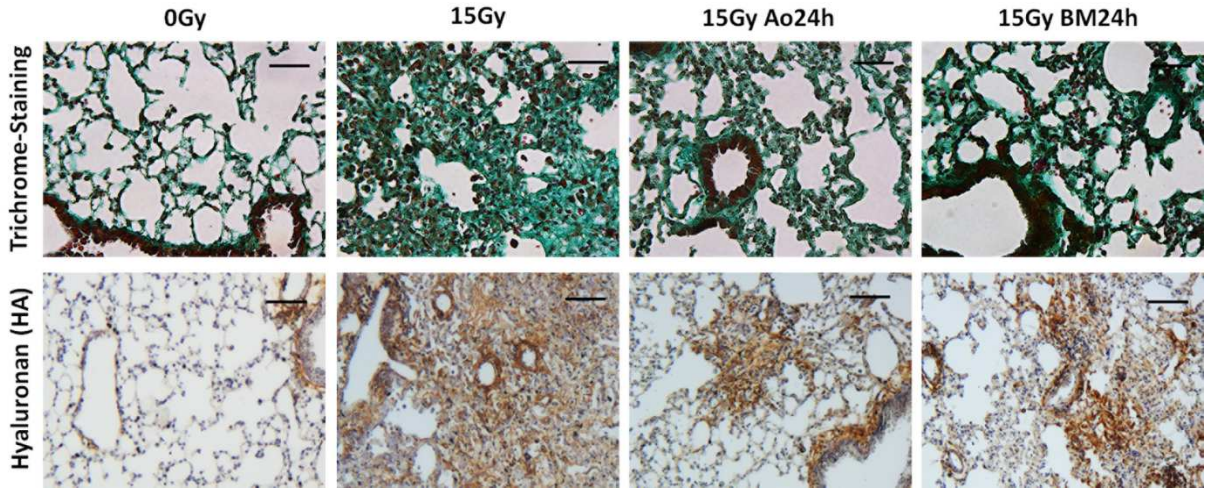

MSC-therapy limits radiation-induced lung fibrosis

C57BL/6 mice were left untreated or received a 15Gy WTI. Single cell suspensions of cultured AoMSCs or BM-MSCs ($0.5*10^6$ cells) were intravenously transplanted into the tail vein of control or WTI mice 24 hours after irradiation. Histological staining with Masson´s Goldner Trichrome on sections of paraffin-embedded lung tissue was performed at 25 weeks after WTI (upper panel, scale bar 15µm). The major extra cellular matrix glycosaminoglycan hyaluronan (HA) was further analyzed in lung section using DAB staining (brown; lower panel; scale bar 25 µm). Shown are representative light microscopy images.

Figure S4

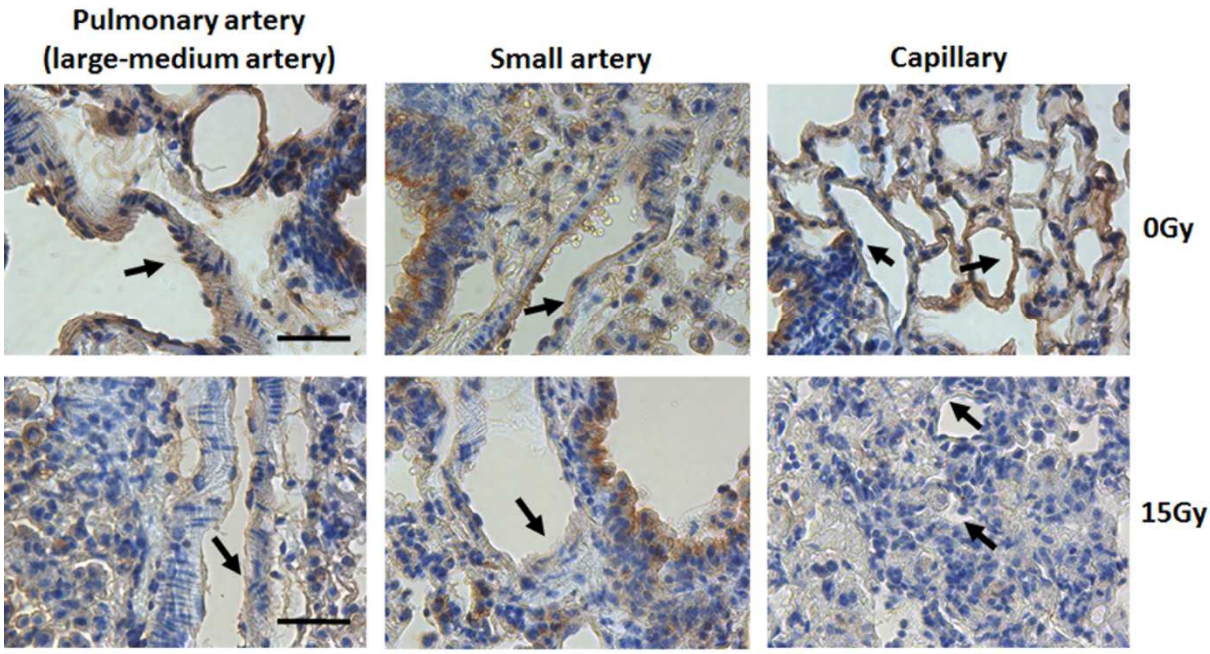

WTI reduces SOD1 expression in lung vessels

C57BL/6 mice were left untreated or received a 15Gy WTI. (A) Lungs were dissected 25 weeks after WTI and subjected to IHC analysis. Vessels were stained for SOD1 using DAB staining (brown). Down-regulation of SOD1 is detected in larger blood vessels (with a thick muscular wall, > 500mm external diameter), in small-sized arteries (with thin muscular wall, up to 100mm in external diameter) and in the microvessels (capillaries) of fibrotic areas. Nuclei were counterstained with Hemalaun (blue). Representative lung photographs are shown. Scale bar 10µm.

Figure S5

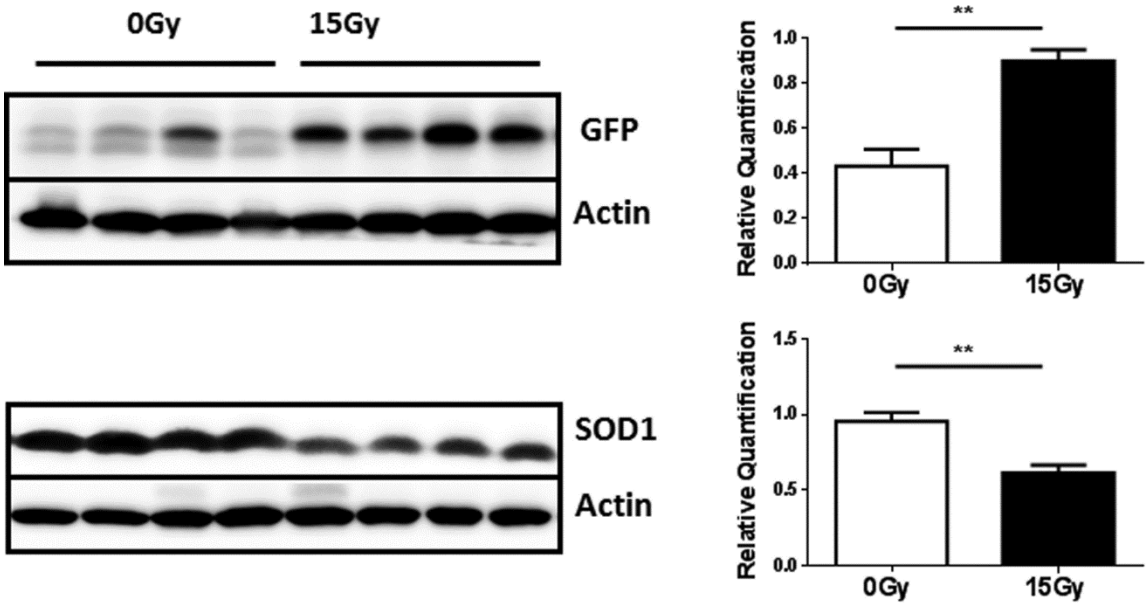

NestGFP(+) MSCs in WTI lungs were affected by ionizing radiation and contribute to fibrosis development

NestGFP mice were left untreated or received a 15Gy WTI. GFP and SOD1 expressions were analyzed in whole protein lysates using Western blot analysis at 25 weeks post irradiation. Representative blots are shown. For quantification blots were analyzed by densitometry and respective GFP and SOD1 signals were related to beta-actin (n=5 for each group). ***P* ≤ 0.01 by one-way ANOVA followed by post-hoc Tukey test.

Supplementary Table 1:

Control supernatants (Ctr) and supernatants derived from cultured aortic (Ao) and bone marrow MSCs (BM) were analyzed by label free quantitative mass spectrometry as described in the method section. Only significantly regulated proteins (as compared to Ctrl) with a fold change >2 and MS/MS counts >25 were listened (FDR 0.05). The minus-signed values imply that proteins are significantly more intense in Ao or BM supernatants as compared to Ctrl supernatants (negative decadic logarithm).

MS/MS Count	-Log t-test p value Ctrl_vs_Ao	t-test Difference Ctrl_vs_Ao	-Log t-test p value Ctrl_vs_BM	t-test Difference Ctrl_vs_BM	Majority protein IDs	Protein names	Gene names
154	2,74	-12,00	2,67	-10,54	Q3TGL4;G5E8B3;P37889-2;P37889	Fibulin-2	Fbln2
61	2,67	-11,67	2,58	-11,22	Q497E4;P68033;P68134	Actin, alpha cardiac muscle 1;Actin, alpha skeletal muscle	Actc1;Acta1
217	2,96	-11,52	2,95	-11,63	P63017;Q504P4	Heat shock cognate 71 kDa protein	Hspa8
181	1,62	-11,34	1,31	-7,77	Q921I1;E9Q035	Serotransferrin	Tf;Gm20425
332	1,64	-11,29	1,53	-9,62	G5E8M2;G5E8B8;G3X9J7;P11276	Fibronectin;Anastellin	Fn1
114	2,20	-11,17	2,19	-10,92	E9PZF0	Nucleoside diphosphate kinase	Gm20390
36	2,37	-11,10	2,35	-10,97	Q9Z0J0	Epididymal secretory protein E1	Npc2
144	2,11	-11,03	2,06	-10,42	P10605	Cathepsin B;Cathepsin B light chain;Cathepsin B heavy chain	Ctsb
251	1,38	-10,98	1,37	-10,85	P26041	Moesin	Msn
139	1,82	-10,95	1,85	-11,27	P35700;B1AXW7	Peroxiredoxin-1	Prdx1
29	2,02	-10,88	1,93	-9,84	P21460;A2APX2;A2APX3	Cystatin-C	Cst3
184	1,30	-10,78	1,30	-10,77	E9PZ00;Q8BFQ1;Q61207;Q3UFE8	Sulfated glycoprotein 1	Psap
104	1,87	-10,65	1,89	-10,88	Q9JII6;Q540D7;B1AXW3	Alcohol dehydrogenase [NADP(+)]	Akr1a1
49	4,76	-10,60	3,76	-8,76	P12032;B1AUP1	Metalloproteinase inhibitor 1	Timp1
63	**2,83**	**-10,46**	**2,89**	**-10,41**	**P08228**	**Superoxide dismutase [Cu-Zn]**	**Sod1**
131	1,42	-10,33	1,40	-10,08	Q3UCD9;P18242;Q8C243	Cathepsin D	Ctsd
156	1,04	-10,33	1,04	-10,37	Q5FWB7;P05064;A6ZI44	Fructose-bisphosphate aldolase	Aldoa;Aldoart1
150	1,77	-10,31	1,79	-10,38	P06745;F6SAC3	Glucose-6-phosphate isomerase	Gpi;Gm1840
99	2,33	-10,26	2,30	-9,86	P28798;Q3U9N4;H3BJE0	Granulins;Acrogranin;Granulin-1	Grn
171	2,50	-10,24	2,46	-9,81	Q80X90	Filamin-B	Flnb

148	3,04	-10,14	3,12	-10,56	Q61598;Q61598-2	Rab GDP dissociation inhibitor beta	Gdi2
36	2,47	-10,14	2,49	-10,61	Q62426	Cystatin-B	Cstb
347	1,22	-10,12	1,26	-10,69	Q61233	Plastin-2	Lcp1
113	1,63	-10,10	1,60	-9,62	P08905	Lysozyme C-2	Lyz2
71	3,37	-10,10	3,36	-10,15	P08249	Malate dehydrogenase, mitochondrial	Mdh2
87	2,67	-10,08	1,95	-9,20	Q5SVY2;P17742;E9Q1E3	Peptidyl-prolyl cis-trans isomerase	Ppia
54	4,21	-10,07	3,45	-8,97	Q6PI17;P25785;B1AQJ3	Metalloproteinase inhibitor 2	Timp2
78	1,30	-10,06	1,31	-10,19	P16045	Galectin-1	Lgals1
102	2,04	-10,01	2,04	-10,09	P68372;Q9D6F9	Tubulin beta-4B chain;Tubulin beta-4A chain	Tubb4b;Tubb4a
138	3,73	-9,94	3,25	-9,72	P27773	Protein disulfide-isomerase A3	Pdia3
54	2,12	-9,94	1,97	-8,44	Q3TNY9;P28653	Biglycan	Bgn
54	3,27	-9,92	3,29	-9,85	P61982;A8IP69	14-3-3 protein gamma;14-3-3 protein gamma, N-terminally processed	Ywhag
122	3,26	-9,90	3,17	-9,93	P05213;P68368	Tubulin alpha-1B chain;Tubulin alpha-4A chain	Tuba1b;Tuba4a
112	2,75	-9,89	2,77	-9,96	Q3U5U6;P14901;H3BKP1	Heme oxygenase 1	Hmox1
247	3,18	-9,86	1,83	-8,49	B7FAU9;Q8BTM8;B7FAV1	Filamin-A	Flna
181	1,42	-9,84	1,24	-8,46	Q64727	Vinculin	Vcl
91	1,26	-9,75	1,29	-10,01	Q5SX50;P62962;Q5SX49	Profilin;Profilin-1	Pfn1
100	2,47	-9,74	2,46	-9,23	Q6IRU2	Tropomyosin alpha-4 chain	Tpm4
42	1,73	-9,67	1,73	-9,62	P10639;A2AV97	Thioredoxin	Txn
67	3,33	-9,67	3,57	-10,10	Q99PT1	Rho GDP-dissociation inhibitor 1	Arhgdia
73	2,60	-9,66	2,78	-9,72	Q9CPX4;P29391;P49945	Ferritin;Ferritin light chain 1;Ferritin light chain 2	Ftl1;Ftl2
85	2,51	-9,66	2,49	-9,36	Q9WVA4	Transgelin-2	Tagln2
52	1,79	-9,64	1,65	-8,24	Q61581;F8WH23;E9Q5D9;F8WII5	Insulin-like growth factor-binding protein 7	Igfbp7
68	2,09	-9,62	2,18	-9,92	Q543K9;P23492	Purine nucleoside phosphorylase	Pnp
124	1,87	-9,61	1,89	-9,64	Q564E2;P06151;G5E8N5	L-lactate dehydrogenase;L-lactate dehydrogenase A chain	Ldha
62	2,32	-9,59	2,21	-8,74	Q62356	Follistatin-related protein 1	Fstl1
75	1,80	-9,54	1,88	-10,34	Q497I3;Q05816;E9Q964	Fatty acid-binding protein, epidermal	Fabp5
126	1,61	-9,50	1,62	-9,54	Q9DBJ1;Q3U7Z6	Phosphoglycerate mutase 1	Pgam1
88	4,29	-9,49	3,82	-9,75	Q99LB4;P24452;D3YTL5	Macrophage-capping protein	Capg

48	2,11	-9,48	2,02	-8,54	Q9QWK4	CD5 antigen-like	Cd5l
128	1,49	-9,47	1,54	-9,92	Q60854;Q4FJQ6;F8WIV2;E9Q096	Serpin B6	Serpinb6
45	2,26	-9,46	2,08	-7,62	Q61646;Q3UBS3	Haptoglobin;Haptoglobin alpha chain;Haptoglobin beta chain	Hp
62	1,36	-9,44	1,35	-9,47	F6TS28;Q8C253;P16110	Galectin-3	Lgals3
157	3,76	-9,43	4,71	-9,65	P40142	Transketolase	Tkt
60	2,16	-9,39	2,18	-9,92	Q61599	Rho GDP-dissociation inhibitor 2	Arhgdib
57	1,51	-9,36	1,55	-9,58	Q5SS40;P62259;D6REF3;F6WA09	14-3-3 protein epsilon	Ywhae
96	1,95	-9,31	1,98	-9,75	Q68FD5;Q5SXR6	Clathrin heavy chain 1	Cltc
81	1,63	-9,27	1,52	-8,10	Q5NCU4;Q5NCU5;P07214	SPARC	Sparc
64	3,38	-9,26	3,15	-9,29	Q5EBQ2;P70296;D3Z1V4	Phosphatidylethanolamine-binding protein 1	Pebp1
61	1,94	-9,26	1,98	-9,29	Q544R6;P16675;G3X8T3	Lysosomal protective protein;Lysosomal protective protein 32 kDa	Ctsa
124	2,81	-9,25	2,77	-8,89	A1BN54;Q7TPR4	Alpha-actinin-1	Actn1
56	1,75	-9,24	1,73	-9,06	Q07797;E9Q5X5	Galectin-3-binding protein	Lgals3bp
30	5,14	-9,22	2,86	-8,96	Q91XJ8;P01887	Beta-2-microglobulin	B2m
33	2,33	-9,20	2,31	-9,11	2;Q60605;E9QLM0	Myosin light polypeptide 6	Myl6
94	2,33	-9,13	3,71	-9,53	P17751;H7BXC3	Triosephosphate isomerase	Tpi1
58	3,18	-9,07	3,04	-7,65	P37804	Transgelin	Tagln
51	1,75	-9,07	1,74	-8,84	Q9D0F9;A2CEK3	Phosphoglucomutase-1	Pgm1;Pgm2
95	3,34	-8,96	3,25	-9,43	Q58E64;P10126;D3YZ68;D3Z3I8	Elongation factor 1-alpha;Elongation factor 1-alpha 1	Eef1a1
114	1,27	-8,95	1,30	-9,32	P09411	Phosphoglycerate kinase 1	Pgk1
65	3,32	-8,93	3,21	-8,99	P99029-2;P99029	Peroxiredoxin-5, mitochondrial	Prdx5
36	2,86	-8,92	3,03	-8,93	F8WJD9;P19157	Glutathione S-transferase P 1	Gstp1
121	2,58	-8,91	2,59	-9,10	Q91VI7	Ribonuclease inhibitor	Rnh1
52	1,31	-8,91	1,53	-10,17	P14152	Malate dehydrogenase, cytoplasmic	Mdh1
71	3,27	-8,87	2,98	-8,99	P15626;D3YX76	Glutathione S-transferase Mu 2	Gstm2
44	1,75	-8,85	1,63	-7,77	Q8C7E4;Q9JJH1	Ribonuclease 4	Rnase4
82	3,23	-8,85	3,26	-9,27	Q99JY9;Q3ULF7	Actin-related protein 3	Actr3
59	3,14	-8,84	4,27	-7,18	G5E899;P22777	Plasminogen activator inhibitor 1	Serpine1
33	2,58	-8,84	2,83	-8,80	P09528	Ferritin heavy chain	Fth1
34	2,01	-8,83	2,03	-8,96	P17047-3;P17047;Q8C5K0	Lysosome-associated membrane glycoprotein 2	Lamp2

76	3,00	-8,79	2,90	-7,70	D3YUK7;Q8CG14;E9Q6C2;E9Q493	Complement C1s-A subcomponent	C1sa;C1s
48	2,00	-8,77	2,06	-9,37	Q8BFR4	N-acetylglucosamine-6-sulfatase	Gns
88	2,25	-8,75	2,19	-8,16	A2AVA0	Sushi, von Willebrand factor type A	Svep1
112	1,77	-8,71	1,77	-8,77	P63101	14-3-3 protein zeta/delta	Ywhaz
68	2,90	-8,71	2,93	-8,30	Q9WUU7;Q545I6;E9Q5W3	Cathepsin Z	Ctsz
47	2,13	-8,70	2,03	-7,84	Q02819;H3BK79	Nucleobindin-1	Nucb1
36	2,47	-8,65	2,47	-8,96	Q99LX0;A2A813;A2A815	Protein DJ-1	Park7
84	2,67	-8,63	1,96	-8,46	P18760;F8WGL3;E9Q1T2	Cofilin-1	Cfl1
30	1,95	-8,58	1,73	-6,51	P28862;Q922W6	Stromelysin-1	Mmp3
60	2,16	-8,51	2,33	-9,31	Q6IR10;P12265	Beta-glucuronidase	Gusb
170	3,54	-8,51	3,55	-8,60	E9Q3W4;E9QK01	Plectin	Plec
86	2,22	-8,51	2,26	-8,93	Q3TW96;F7AWB4;Q3TW96-2	UDP-N-acetylhexosamine pyrophosphorylase-like protein 1	Uap1l1
174	1,41	-8,50	1,55	-9,41	P58252	Elongation factor 2	Eef2
65	2,83	-8,49	3,19	-9,07	Q9R0P3;H3BKH6	S-formylglutathione hydrolase	Esd
56	3,63	-8,47	2,74	-8,58	Q6ZWX2;P20065-2;P20065;A2AHI6	Thymosin beta-4;Hematopoietic system regulatory peptide	Tmsb4x
25	2,60	-8,43	1,99	-8,16	P50543;G5E8Y7	Protein S100-A11	S100a11
42	2,05	-8,42	2,12	-9,10	Q9WV54;Q78P93	Acid ceramidase;Acid ceramidase subunit alpha	Asah1
43	3,31	-8,41	3,07	-8,92	P00493;B1B0W8	Hypoxanthine-guanine phosphoribosyltransferase	Hprt1
84	1,99	-8,40	1,92	-7,64	Q3UG07;P33434	72 kDa type IV collagenase;PEX	Mmp2
39	2,76	-8,35	2,60	-7,18	Q640N1;Q640N1-2	Adipocyte enhancer-binding protein 1	Aebp1
46	2,56	-8,32	2,47	-8,52	Q9CQV8;A2A5N2	14-3-3 protein beta/alpha;14-3-3 protein beta/alpha	Ywhab
101	2,98	-8,32	2,93	-7,82	A2AQ53;Q61554	Fibrillin-1	Fbn1
105	2,17	-8,28	2,14	-8,09	Q8VDD5	Myosin-9	Myh9
43	1,83	-8,26	2,19	-8,08	Q61792;Q543N3	LIM and SH3 domain protein 1	Lasp1
25	1,86	-8,26	1,82	-7,96	Q60648;Q5F1Z8	Ganglioside GM2 activator	Gm2a
30	2,73	-8,26	2,78	-8,63	Q8BVA0;Q99P91	Transmembrane glycoprotein NMB	Gpnmb
62	2,50	-8,25	2,33	-6,77	P07141;P07141-2;D3Z090	Macrophage colony-stimulating factor 1	Csf1
26	2,87	-8,24	2,65	-8,08	P63028	Translationally-controlled tumor protein	Tpt1
44	3,25	-8,23	2,98	-7,47	Q91X24;P47880	Insulin-like growth factor-binding protein 6	Igfbp6
64	2,76	-8,22	2,63	-7,76	P09103	Protein disulfide-isomerase	P4hb

28	2,56	-8,18	2,77	-8,19	P26883;A2AT05;Q3UKJ3;F6X9I3	Peptidyl-prolyl cis-trans isomerase FKBP1A	Fkbp1a
53	1,45	-8,17	1,47	-8,34	Q61171;D3Z4A4	Peroxiredoxin-2	Prdx2
44	1,76	-8,14	1,80	-8,62	Q93092	Transaldolase	Taldo1
31	1,85	-8,14	1,75	-7,34	Q3UPN1;P29533;Q544V4;P29533-2	Vascular cell adhesion protein 1	Vcam1
57	3,34	-8,14	2,92	-8,85	Q62465;Q499X4	Synaptic vesicle membrane protein VAT-1 homolog	Vat1
35	1,83	-8,12	1,76	-7,43	P10493	Nidogen-1	Nid1
72	4,29	-8,11	4,15	-8,77	O88844;F8WIY0	Isocitrate dehydrogenase [NADP] cytoplasmic	Idh1
65	1,79	-8,10	1,88	-9,23	Q3TXU4;P08226;G3UWN5	Apolipoprotein E	Apoe
47	3,48	-8,09	3,20	-7,57	Q8BPB5;E9Q582	EGF-containing fibulin-like extracellular matrix protein 1	Efemp1
45	1,08	-8,08	1,12	-8,49	Q9CQI6;Q544F6	Coactosin-like protein	Cotl1
37	1,80	-8,07	1,78	-7,63	Q61398;Q3UIP2	Procollagen C-endopeptidase enhancer 1	Pcolce
35	2,44	-8,04	2,42	-8,07	P05202	Aspartate aminotransferase, mitochondrial	Got2
35	3,16	-8,04	3,13	-8,29	Q9CQ60;Q8CBG6;D3Z4X1;F6X8L5	6-phosphogluconolactonase	Pgls
46	2,10	-8,03	1,99	-7,12	E9PX70;Q60847-25;Q60847	Collagen alpha-1(XII) chain	Col12a1
37	1,83	-8,02	1,87	-8,33	P68254-2;P68254;A3KML3	14-3-3 protein theta	Ywhaq
124	1,28	-8,01	1,33	-8,45	Q3TJY2;O88342	WD repeat-containing protein 1	Wdr1
124	1,60	-8,01	1,58	-7,77	Q99K51;B1AX58	Plastin-3	Pls3
36	1,90	-7,99	1,87	-8,07	Q9R0P5;Q4FK36	Destrin	Dstn
39	2,63	-7,99	2,59	-8,48	Q91VW3	SH3 domain-binding glutamic acid-rich-like protein 3	Sh3bgrl3
38	2,11	-7,98	2,06	-7,61	O09131	Glutathione S-transferase omega-1	Gsto1
38	3,62	-7,96	4,01	-7,48	Q3TUF3;O35887;Q6XLQ8	Calumenin	Calu
36	3,11	-7,96	2,63	-7,51	Q9DCY1;P24369	Peptidyl-prolyl cis-trans isomerase	Ppib
32	3,23	-7,94	3,41	-7,89	P62774	Myotrophin	Mtpn
64	3,82	-7,93	4,05	-8,27	F6U106;O88569;O88569-3	Heterogeneous nuclear ribonucleoproteins A2/B1	Hnrnpa2b1
71	2,31	-7,92	2,35	-8,32	Q9JKF1;G3UW45;F6ZJB0	Ras GTPase-activating-like protein IQGAP1	Iqgap1
52	3,89	-7,90	3,50	-7,56	P20029;A2AUF6	78 kDa glucose-regulated protein	Hspa5
54	2,31	-7,89	2,35	-8,23	Q923G3;P47757-2;A2AMW0	F-actin-capping protein subunit beta	Capzb
27	3,45	-7,85	2,90	-7,62	Q9CPU0;A5GZX3	Lactoylglutathione lyase	Glo1
41	2,42	-7,80	2,46	-8,60	Q5SW83;P61161	Actin-related protein 2	Actr2
60	2,61	-7,79	2,58	-7,46	Q8VHX6-2;D3YW87;Q8VHX6	Filamin-C	Flnc

40	2,09	-7,78	2,09	-8,24	Q3TXR9;P20060	Beta-hexosaminidase;Beta-hexosaminidase subunit beta	Hexb
266	1,04	-7,78	1,03	-7,16	P26039;F8WGT0	Talin-1	Tln1
46	1,43	-7,74	1,40	-7,45	Q9CPY7-2;Q9CPY7	Cytosol aminopeptidase	Lap3
56	3,38	-7,74	3,08	-7,85	P19324	Serpin H1	Serpinh1
25	2,08	-7,71	2,55	-6,00	Q03366;A9Z1Z1	C-C motif chemokine 7	Ccl7
26	1,85	-7,69	1,89	-8,14	Q91YR1	Twinfilin-1	Twf1
33	3,52	-7,68	3,24	-6,63	Q61508;Q61508-2	Extracellular matrix protein 1	Ecm1
83	1,07	-7,68	1,24	-8,93	Q9DCD0;A2AH73	6-phosphogluconate dehydrogenase, decarboxylating	Pgd
38	2,27	-7,64	2,33	-7,92	Q8K354	Carbonyl reductase [NADPH] 3	Cbr3
31	3,76	-7,62	3,21	-7,24	Q80ZP8;Q3TMX5;Q9CXI5	Mesencephalic astrocyte-derived neurotrophic factor	Manf
28	1,59	-7,62	1,57	-7,10	Q3TC45;P08207	Protein S100-A10	S100a10
42	2,41	-7,62	2,49	-8,09	Q3UDY1;P45376;G3UW73	Aldose reductase	Akr1b3;Akr1b1
37	3,09	-7,61	2,94	-7,61	Q9CPV4;Q9CPV4-3;E9Q197	Glyoxalase domain-containing protein 4	Glod4
29	3,05	-7,60	2,59	-8,07	P05201	Aspartate aminotransferase, cytoplasmic	Got1
35	2,78	-7,58	2,86	-7,99	Q4FJX9;P09671	Superoxide dismutase;Superoxide dismutase [Mn]	Sod2
35	3,25	-7,58	3,34	-7,83	P14206;D3YTT7	40S ribosomal protein SA	Rpsa;Rpsa-ps10
121	1,68	-7,58	2,01	-8,44	P16858;D2KHZ9	Glyceraldehyde-3-phosphate dehydrogenase	Gapdh;Gm7293;Gm631
51	2,97	-7,56	2,70	-7,47	P50396	Rab GDP dissociation inhibitor alpha	Gdi1
33	1,78	-7,46	1,81	-7,78	E9PX84;Q3TRE6;P98078-3	Disabled homolog 2	Dab2
40	3,10	-7,45	2,93	-7,91	Q9CVB6;D3YXG6	Actin-related protein 2/3 complex subunit 2	Arpc2
41	3,01	-7,44	3,33	-7,87	P29416;E9PW67	Beta-hexosaminidase subunit alpha	Hexa
43	1,66	-7,43	1,71	-7,98	O54782	Epididymis-specific alpha-mannosidase	Man2b2
34	3,35	-7,43	3,34	-7,75	Q9R062;Q3TWR9;D3Z5N4	Glycogenin-1	Gyg1;Gyg
32	2,99	-7,42	3,04	-7,72	Q9DBP5	UMP-CMP kinase	Cmpk1
56	2,67	-7,42	2,61	-7,05	P48678;B3RH23	Prelamin-A/C;Lamin-A/C	Lmna
43	1,37	-7,40	1,35	-7,38	P62204;Q3UKW2	Calmodulin	Calm1
33	2,03	-7,40	2,10	-8,06	Q9WV32	Actin-related protein 2/3 complex subunit 1B	Arpc1b
47	1,94	-7,37	1,98	-7,74	Q3U4W8;P56399	Ubiquitin carboxyl-terminal hydrolase	Usp5
33	1,68	-7,35	1,69	-7,56	Q3U4U6;P80318	T-complex protein 1 subunit gamma	Cct3
70	1,57	-7,34	1,61	-7,73	Q02053;B9EHN0	Ubiquitin-like modifier-activating enzyme 1	Uba1

170	1,02	-7,32	1,23	-9,47	Q9D1A2;F6XEL6	Cytosolic non-specific dipeptidase	Cndp2
65	2,96	-7,29	3,19	-7,74	Q61830;Q2HZ94	Macrophage mannose receptor 1	Mrc1
37	2,09	-7,25	1,96	-6,36	Q8CG16;F6QBW6	Complement C1r-A subcomponent	C1ra;C1rb
235	2,22	-7,24	2,32	-7,56	P52480-2	Pyruvate kinase PKM	Pkm
62	2,98	-7,22	3,45	-7,61	Q3U2G2;Q61316	Heat shock 70 kDa protein 4	Hspa4
67	1,75	-7,17	1,80	-7,67	Q8K183;D3Z7R1	Pyridoxal kinase	Pdxk
42	2,27	-7,15	2,23	-7,80	Q3TAW7;P23780;E9PVK3;F7AF87	Beta-galactosidase	Glb1
51	1,47	-7,14	1,53	-7,76	P10649;A2AE89;F6WHQ7	Glutathione S-transferase Mu 1	Gstm1
45	2,58	-7,11	2,73	-8,00	Q9D8U8;A2ANA4	Sorting nexin-5	Snx5
59	1,41	-7,10	1,50	-7,77	P50516;P50516-2	V-type proton ATPase catalytic subunit A	Atp6v1a
40	1,45	-7,08	1,39	-5,88	Q543M3;P06797	Cathepsin L1;Cathepsin L1 heavy chain;Cathepsin L1 light chain	Ctsl;Ctsl1
44	2,11	-7,05	2,11	-7,13	Q9WU78;Q9WU78-3;B8JJL8	Programmed cell death 6-interacting protein	Pdcd6ip
31	2,37	-7,02	2,42	-7,30	P50428	Arylsulfatase A	Arsa
27	2,52	-6,99	2,92	-7,19	P24527	Leukotriene A-4 hydrolase	Lta4h
38	2,05	-6,97	2,12	-7,52	Q9Z1Q5;Q542F1	Chloride intracellular channel protein 1	Clic1
113	0,91	-6,96	0,86	-6,26	Q01853	Transitional endoplasmic reticulum ATPase	Vcp
25	1,50	-6,96	1,52	-7,04	Q91ZJ5	UTP--glucose-1-phosphate uridylyltransferase	Ugp2
419	2,05	-6,95	2,07	-7,17	Q4KL81;P63260;F8WI82;E9Q607	Actin, cytoplasmic 2;Actin, cytoplasmic 2, N-terminally processed	Actg1
40	2,11	-6,93	2,09	-6,71	Q9R111;Q548F2;D3YU09	Guanine deaminase	Gda
34	2,87	-6,92	3,02	-7,72	Q3U1N0;O89053;G3UYK8	Coronin;Coronin-1A	Coro1a
26	2,06	-6,90	2,30	-7,16	Q9R1P0;E9PW69;E9Q0X0	Proteasome subunit alpha type-4;Proteasome subunit alpha type	Psma4
46	3,25	-6,88	3,25	-6,78	Q91ZX7	Prolow-density lipoprotein receptor-related protein 1	Lrp1
161	2,09	-6,87	2,11	-6,98	Q5FW97;P17182;Q6PHC1	Alpha-enolase;Enolase	Eno1
75	1,79	-6,87	1,81	-6,85	P27546-2;P27546	Microtubule-associated protein 4;Microtubule-associated protein	Map4
30	2,05	-6,84	1,97	-6,26	Q8CI51;Q8CI51-2	PDZ and LIM domain protein 5	Pdlim5
64	1,01	-6,81	0,82	-4,90	B1B0C7;E9PZ16;E9QL02	Basement membrane-specific heparan sulfate proteoglycan core	Hspg2
46	2,81	-6,81	2,86	-7,37	Q9JM76;H7BWZ3;D3Z2F7;D3Z2F8	Actin-related protein 2/3 complex subunit 3	Arpc3
37	2,53	-6,81	2,32	-6,89	P57759	Endoplasmic reticulum resident protein 29	Erp29
25	2,31	-6,81	2,32	-7,02	P60335	Poly(rC)-binding protein 1	Pcbp1
203	0,75	-6,79	0,68	-6,05	Q3ULT2;P57780;E9Q2W9	Alpha-actinin-4	Actn4

29	2,63	-6,73	2,67	-7,25	Q78ZM0;D3Z789;D3Z6Z0;O70492	Sorting nexin-3	Snx3
42	2,21	-6,72	2,26	-6,93	Q9D154	Leukocyte elastase inhibitor A	Serpinb1a
46	1,42	-6,71	1,37	-6,47	Q9Z2W0;Q8BPW9	Aspartyl aminopeptidase	Dnpep
34	3,18	-6,70	2,71	-6,40	Q61553	Fascin	Fscn1
31	1,80	-6,70	1,85	-7,08	O09159	Lysosomal alpha-mannosidase	Man2b1
33	3,53	-6,68	3,37	-6,67	Q9Z2U1;Q3UPK6;D3YX79	Proteasome subunit alpha type-5;Proteasome subunit alpha type	Psma5;Gm8394
31	2,02	-6,68	2,09	-7,37	P56480	ATP synthase subunit beta, mitochondrial	Atp5b
66	1,93	-6,67	2,04	-7,33	Q3TCN2;Q3TCN2-2	Putative phospholipase B-like 2	Plbd2
94	1,27	-6,67	1,11	-5,47	Q3TX57;Q01149;E9Q6U9	Collagen alpha-2(I) chain	Col1a2
26	1,93	-6,66	1,94	-6,78	Q11136;A2RS23	Xaa-Pro dipeptidase	Pepd
32	2,77	-6,58	2,80	-6,74	Q8R016;E9PY26	Bleomycin hydrolase	Blmh
33	3,48	-6,58	3,47	-6,69	Q3UL22;P42932;H3BL49;H3BJB6	T-complex protein 1 subunit theta	Cct8
25	1,80	-6,52	1,85	-6,69	P61089;A2RTT4	Ubiquitin-conjugating enzyme E2 N	Ube2n
26	1,34	-6,51	1,36	-6,61	Q99KJ8;Q3TPZ5	Dynactin subunit 2	Dctn2
43	2,20	-6,49	2,23	-6,41	Q00519	Xanthine dehydrogenase/oxidase	Xdh
28	2,90	-6,48	2,86	-6,78	Q9JJU8	SH3 domain-binding glutamic acid-rich-like protein	Sh3bgrl
50	2,65	-6,48	2,67	-6,82	Q99KC8	von Willebrand factor A domain-containing protein 5A	Vwa5a
120	1,68	-6,43	1,93	-8,64	O08553	Dihydropyrimidinase-related protein 2	Dpysl2
65	2,33	-6,43	2,35	-6,65	Q9JHU4	Cytoplasmic dynein 1 heavy chain 1	Dync1h1
25	2,78	-6,42	2,78	-6,47	D3YWF6;Q7TQI3	Ubiquitin thioesterase OTUB1	Otub1
28	2,74	-6,37	2,91	-7,06	Q9WUM3;A2RS22	Coronin-1B;Coronin	Coro1b
28	1,57	-6,31	1,59	-6,03	P26043;Q3U111;Q7TSG6	Radixin	Rdx
30	1,99	-6,31	1,98	-6,21	Q3TML0;Q922R8	Protein disulfide-isomerase A6	Pdia6
25	2,51	-6,30	2,28	-5,30	Q62009-5;Q62009-3	Periostin	Postn
33	3,41	-6,28	3,45	-7,00	Q571E4;Q8CC47	N-acetylgalactosamine-6-sulfatase	Galns
34	2,36	-6,22	2,33	-5,91	Q3UKR1;P28654	Decorin	Dcn
25	2,43	-6,21	2,56	-5,95	O70400	PDZ and LIM domain protein 1	Pdlim1
26	2,86	-6,20	3,05	-6,92	Q9WUM4;Q499X7	Coronin-1C;Coronin	Coro1c
92	1,60	-6,19	1,49	-5,92	Q04447	Creatine kinase B-type	Ckb
43	1,31	-6,18	1,32	-6,77	O70370;Q3UD32	Cathepsin S	Ctss

26	2,21	-6,15	2,18	-5,98	Q8R1F1	Niban-like protein 1	Fam129b
290	4,47	-6,14	4,62	-6,41	Q5FWJ3;P20152;E9PZV5	Vimentin	Vim
48	2,35	-6,13	2,26	-6,39	P70699;A2AFL4	Lysosomal alpha-glucosidase	Gaa
25	1,84	-6,09	1,78	-5,46	P14211;B2MWM9	Calreticulin	Calr
25	3,65	-6,09	3,23	-6,40	Q561N4;P68037;D3YZS3	Ubiquitin-conjugating enzyme E2 L3	Ube2l3
26	1,45	-5,99	1,50	-6,36	Q9D031;Q01730;A2AUR7	Ras suppressor protein 1	Rsu1
33	1,72	-5,96	1,70	-5,54	O88968	Transcobalamin-2	Tcn2
26	3,44	-5,95	3,25	-4,71	Q542X9;O09164	Superoxide dismutase [Cu-Zn]	Sod3
76	0,98	-5,94	0,99	-6,02	Q6GT24;O08709;D3Z0Y2	Peroxiredoxin-6	Prdx6
44	2,67	-5,92	3,40	-6,74	Q790Y8;Q00612;A3KG36	Glucose-6-phosphate 1-dehydrogenase	G6pdx
38	2,28	-5,87	2,33	-6,11	P80316	T-complex protein 1 subunit epsilon	Cct5
31	1,87	-5,87	1,94	-6,20	Q542X7;P80314	T-complex protein 1 subunit beta	Cct2
121	1,96	-5,84	1,91	-4,99	Q5ND38;P97298;B7ZC25	Pigment epithelium-derived factor	Serpinf1
32	2,04	-5,79	2,03	-5,59	Q7TQE2;Q62523;E9Q625	Zyxin	Zyx
31	1,54	-5,72	1,65	-6,49	Q9EQH3;Q3TRJ1	Vacuolar protein sorting-associated protein 35	Vps35
25	2,33	-5,71	2,45	-5,67	E9Q1S3;Q01405	Protein transport protein Sec23A	Sec23a
174	1,26	-5,68	1,31	-6,03	Q6PAC1;P13020-2	Gelsolin	Gsn
61	2,48	-5,65	2,48	-5,66	P16546-2;P16546;A3KGU5	Spectrin alpha chain, non-erythrocytic 1	Sptan1
36	2,37	-5,60	2,46	-6,42	P29351;Q3UCJ0;P29351-2	Tyrosine-protein phosphatase non-receptor type 6	Ptpn6
25	3,61	-5,60	3,38	-5,09	P02463	Collagen alpha-1(IV) chain;Arresten	Col4a1
29	2,12	-5,56	2,17	-5,80	P11983;P11983-2	T-complex protein 1 subunit alpha	Tcp1
43	2,01	-5,54	2,09	-6,02	P62814	V-type proton ATPase subunit B, brain isoform	Atp6v1b2
35	1,88	-5,53	1,93	-5,76	Q99KK7	Dipeptidyl peptidase 3	Dpp3
33	1,76	-5,49	1,72	-5,44	Q9QYB1;Q543N5	Chloride intracellular channel protein 4	Clic4
38	0,88	-5,47	0,90	-5,61	Q6ZWZ6;P63323;D3Z6B6;D3Z1P4	40S ribosomal protein S12	Rps12
26	2,62	-5,40	2,31	-5,72	P62827;Q14AA6	GTP-binding nuclear protein Ran	Ran;1700009N14Rik
29	2,01	-5,35	2,07	-5,62	Q8BL66;E9PWF5	Early endosome antigen 1	Eea1
32	1,91	-5,33	1,93	-5,52	Q9CWJ9	Bifunctional purine biosynthesis protein PURH	Atic
31	1,92	-5,31	2,04	-6,05	Q61425	Hydroxyacyl-coenzyme A dehydrogenase, mitochondrial	Hadh
33	2,04	-5,29	1,95	-5,44	Q543N6;P58389;A2AWE9	Serine/threonine-protein phosphatase 2A activator	Ppp2r4

25	2,72	-5,27	2,68	-5,26	Q9CQM9	Glutaredoxin-3	Glrx3
25	2,53	-5,23	2,44	-5,67	Q9DBG3;Q9DBG3-2;Q5SWR1	AP-2 complex subunit beta	Ap2b1
176	0,57	-5,21	0,64	-5,85	P40124	Adenylyl cyclase-associated protein 1	Cap1
39	1,69	-5,05	1,75	-5,30	P19096	Fatty acid synthase;[Acyl-carrier-protein] S-acetyltransferase	Fasn
39	1,95	-4,86	2,22	-4,63	Q91XV3	Brain acid soluble protein 1	Basp1
25	2,38	-4,81	2,56	-5,66	P17439	Glucosylceramidase	Gba
78	1,71	-4,80	1,66	-4,69	Q80YQ1;P35441	Thrombospondin-1	Thbs1
33	1,19	-4,74	1,17	-4,29	Q921U7;Q8CE04;P51125-7	Calpastatin	Cast
25	2,61	-4,70	2,68	-5,06	E9Q8S8;Q3TRM8;E9Q3Z4	Hexokinase-3	Hk3
207	2,21	-4,63	1,96	-3,35	P01027	Complement C3	C3
49	1,82	-4,49	1,74	-4,05	F6SIG2;Q3TVI5;P08121;Q5DTG2	Collagen alpha-1(III) chain	Col3a1
32	1,60	-4,48	1,72	-4,71	Q9DBG5	Perilipin-3	Plin3
33	1,53	-4,24	1,57	-4,29	Q03350;F8WHK2	Thrombospondin-2	Thbs2
26	0,86	-4,12	1,12	-6,35	Q8BH61	Coagulation factor XIII A chain	F13a1
54	1,46	-4,08	1,87	-6,62	Q923D2;Q3U6G1;E9PZC3	Flavin reductase (NADPH)	Blvrb
63	1,52	-4,01	1,13	-2,49	P11087;P11087-2;F8WGB7	Collagen alpha-1(I) chain	Col1a1